Title

HemK2 functions for sufficient protein synthesis and RNA stability through eRF1 methylation during Drosophila oogenesis

Authors

Fengmei Xu[1], Ritsuko Suyama[1], Toshifumi Inada[2], Shinichi Kawaguchi[1]*, and Toshie Kai[1]*

*Corresponding author

E-mail: kawaguchi.shinichi.fbs@osaka-u.ac.jp (KS)

E-mail: kai.toshie.fbs@osaka-u.ac.jp (KT)

Affiliations

[1] Graduate School of Frontier Biosciences, Osaka University, Osaka 565-0871, Japan

[2] Division of RNA and Gene regulation, Institute of Medical Science, The University of Tokyo, Tokyo 108-8639, Japan.

Abstract

HemK2 is a well-conserved methyltransferase from yeast to human, but genuine substrates remain controversial, and its biological significance in the higher organism remains elusive. In this study, we report HemK2 functions for the methylation of eukaryotic Release Factor 1 (eRF1), which is required for female germline development in *Drosophila melanogaster.* Germline-knockdown of *hemk2* (*hemk2*-GLKD) causes apoptosis of germline cells, and severe downregulation of eRF1 methylation and protein synthesis. Overexpression of methylation-deficient eRF1 phenocopies the defects observed in *hemk2*-GLKD, suggesting that eRF1 is the primary substrate for methylation by HemK2. We show that *hemk2*-GLKD also results in significant downregulation of mRNAs in germline cells, and the defects in egg formation and protein synthesis are partially rescued by blocking the no-go decay pathway. In addition, *hemk2* knockdown increases disome formation, suggesting that perturbation of eRF1 methylation results in ribosome stalling, which in turn triggers ribosome quality control to degrade actively translated mRNAs. We propose that eRF1 methylation by HemK2 is required for the efficient protein production and mRNA stability, to ensure the formation of the high-quality eggs.

Introduction

Post-translational modifications (PTMs), such as methylation phosphorylation, glycosylation, acetylation, and ubiquitination, are chemical alterations occurring after protein synthesis. PTMs significantly impact protein functions, interactions, stability, and enzymatic activity (Ramazi and Zahiri, 2021; Ryšlavá et al., 2013). Among those over 400 types of different PTMs, methylation is one of the most widespread modifications. Methylation reaction is catalyzed by S-adenosylmethionine-dependent methyltransferases (MTases), transferring methyl groups to various biomolecules, not only to proteins but also to DNA and RNA at their cytosines and adenines (Chen et al., 2013; Dai et al., 2021; Ping et al., 2014; Wang et al., 2016). In *Drosophila* genome, 127 MTase genes have been annotated. These MTases were further categorized based on their substrate specificities. Lysine MTases and arginine MTases form large group in protein MTases. Previous studies on histone methylation have highlighted the significance of lysine/arginine modifications in transcription regulation (Gates et al., 2017; Zhao and Garcia, 2015). Besides lysine and arginine residues, however, other amino acid residues such as histidine (Clarke, 2013), aspartic acid (Sprung et al., 2008), asparagine (Klotz et al., 1990), and glutamine (Heurgué-Hamard et al., 2002) are also known to undergo a methylation.

HemK2 is a member of unclassified protein MTases because the different classes of substrates are known to this MTase. HemK2 has been previously

reported to catalyze methylation of histone H4 lysine 12 (H4K12), DNA N6-adenine (6mA) and eukaryotic translation release factor 1 (eRF1). HemK2-mediated histone H4K12 methylation regulates the proliferation of prostate tumor cells (Metzger et al., 2019), while reduced genomic DNA 6mA levels are associated with tumorigenesis in cancer patients (Xiao et al., 2018). However, the enzymatic activity of HemK2 towards genomic DNA 6mA remains controversial (Kweon et al., 2019; Ratel et al., 2006; Woodcock et al., 2019). On the other hand, the role of HemK2 as a MTase for eRF1 has been well studied in yeast and mammalian culture cells. HemK2 (N6AMT1 in humans; YDR140w or Mtq2p in yeast) methylates the glutamine residue in the GGQ motif of eRF1 (Figaro et al., 2008; Heurgué-Hamard et al., 2006; Liu et al., 2010). Depletion of HemK2 in yeast (Mtq2p) resulted in sensitivity to translation fidelity of antibiotics (Polevoda et al., 2006). Mouse HemK2 (PRED28) deficiency led to early embryonic lethality and impaired post implantation development (Liu et al., 2010). However, whether these potential substrates are methylated by HemK2 in the physiological conditions in multicellular animals remains unclear.

Drosophila oogenesis is an ideal model for studying genetic regulation of egg production. The female contains a pair of ovaries, each of which consist of 18–20 ovarioles containing the germarium at the anterior tip followed by progressively developing egg chambers (Avilés-Pagán and Orr-Weaver, 2018; Gleason et al., 2018; Rastegari et al., 2020). Each egg chamber contains one

oocyte and 15 nurse cells which support oocyte growth and is surrounded by a monolayer of somatic follicle cells. Successful accomplishment of processes such as stem cell maintenance, their asymmetric division and differentiation, meiosis, and more importantly, the production of mRNAs and proteins to be maternally deposited to eggs, is crucial for proper oogenesis. *Drosophila* oogenesis is an energetically consuming process involving cellular proliferation and growth that requires diverse protein synthesis (Lasko, 2012).

The role of HemK2 as a MTase has been well studied in yeast and mammalian culture cells. However, its function in animals, especially in the reproductive system where active gene expression and protein medication take place, remains unclear. Here, we characterized HemK2's role in eRF1 methylation during *Drosophila* oogenesis. HemK2 was essential for egg production; upon knocking down of *hemk2* expression, oogenesis stopped in the mid stage and germline cells were degenerated by apoptosis. Perturbation of *hemk2* expression caused severe reduction of eRF1 methylation but not DNA 6mA and H4K12 methylation. Furthermore, ineffective termination resulting from unmethylated eRF1 also decreased mRNA abundance through the No-go-decay pathway. Taken together, these results suggest an essential role of *hemk2*-mediated eRF1 methylation in ensuring efficient protein production and mRNA stability, thereby regulating gene expression during *Drosophila* oogenesis.

Results

Germline knockdown of *hemk2* exhibited female sterility marked by the developmental arrest in the mid-oogenesis

To explore function of a well-conserved methyltransferase, HemK2, encoded by *CG9960* in *Drosophila melanogaster*, we knocked down its expression by driving shRNA targeting its 3'UTR (BL#40837) with a germline driver, *NGT40; NosGal4-VP16* (Grieder et al., 2000). The oocyte starts accumulating proteins and RNAs provided by 15 nurse cells through the cytoplasmic channels (Figure 1A, B). The females subjected to germline-knockdown of *hemk2* (*hemk2*-GLKD), which resulted in ~65% of reduction of its mRNA level (Figure 1C, S1A), exhibited female sterility. *hemk2*-GLKD females contained small ovaries and did not lay any eggs at all (Figure 1B, D), suggesting the developmental arrest of egg chambers at stages 7/8 prior to the vitellogenic stages. In contrast, *hemk2*-GLKD males with ~75% reduction in the mRNA level did not show any significant defects in fertility (Figure S1F, G).

hemk2 expression is under di-cistronic control, being co-expressed as a single transcript along with the other open reading frame, *snapin*, in the upstream of the *hemk2* coding frame (Figure S1A) (Wall et al., 2005). In order to verify if the defects in *hemk2*-GLKD were caused by reduction of *hemk2* expression, each single transgene of N-terminal FLAG-tagged HemK2 or

Snapin devoid of shRNA targeting sequence was expressed in germline upon the knockdown of the di-cistronic transcript (Figure 1E; Figure S1E). The number of laid eggs and hatching rate in the females expressing *hemk2* in germline were comparable with those of the control (Figure 1D), indicating that the defect was rescued. In contrast, the *snapin* expression did not recover those defects (Figure S1D). These results indicate the female sterility was caused by the deterioration of *hemk2* function upon the knocking down of the dicistronic transcript, and *hemk2* had essential roles in germline cells during oogenesis.

To investigate *hemk2*'s function in somatic cells, *hemk2* was knocked down in ovarian somatic cells including follicle cells by a somatic driver, *traffic jam-Gal4 (tj-Gal4)*. Upon *hemk2* somatic-knockdown (*hemk2*-STKD), the females became sterile, and the ovaries were rudimentary (Figure S1B, C). *hemk2*-STKD ovaries often contained the fused egg chambers and disorganized follicle cells (Figure S1C). The fertility and developmental defects were almost completely rescued by the expression of *hemk2* transgene by *tj-Gal4* (Figure S1B, C), suggesting that *hemk2* has a predominant role not only in germline but also in somatic cells.

hemk2-GLKD ovaries showed pleiotropic phenotypes: hyperplasia of the posterior follicle cells, failure in chromosome dispersion, and massive apoptosis of germline cells (Figure 2). While all the egg chambers in the control females were encapsulated by a monolayer of follicle cells, those in

most of *hemk2*-GLKD ovarioles contained multiple layered follicle cells at the posterior region (Figure 2A; 94 %). Moreover, cells positive for phospho-histone H3 (pH3), a marker of mitosis, were often enriched within the multi-layered follicle cells of *hemk2*-GLKD during stage 7/8 (Figure 2A), indicating their hyperplasia at posterior side of egg chambers.

Secondly, *hemk2*-GLKD nurse cells showed a chromosome dispersion defect. The wildtype nurse cells in early oogenesis form polytene chromosomes condensing into a characteristic ‘5-blob’ conformation and become dispersed completely by stage 6 (Dej and Spradling, 1999). However, almost all ovarioles of *hemk2*-GLKD harbored nurse cell nuclei containing chromosomes remained in a blob-like configuration even beyond stage 6 (Figure 2B, Figure S2A; 99%). In order to investigate the possible causes that may results in this chromosomal defect, we examined the expression level of the genes which were known to function for chromosomal dispersion (Goodrich et al., 2004; Klusza et al., 2013). Among those genes, qRT-PCR analysis revealed that the mRNA level of *otu* was most drastically reduced upon *hemk2*-GLKD (Figure 2C), suggesting a potential correlation between *otu* expression and the observed defect. The expression of N-terminal FLAG-tagged Otu104 isoform in *hemk2*-GLKD ovaries significantly restored the number of ovarioles containing dispersed chromosomes (Figure S2A). These results suggest that *hemk*2 functions for the chromosome dispersion during oogenesis, at least in part, by ensuring the expression of *otu*.

Thirdly, *hemK2*-GLKD resulted in massive degeneration of egg chambers in mid-oogenesis where the germline cell death led to degeneration of egg chambers depending on physiological conditions and environmental cues as a developmental checkpoint (Drummond-Barbosa and Spradling, 2001; McCall, 2004). Immunostaining of *hemk2*-GLKD with antibody against p53, an inducer of apoptosis, revealed increased accumulation of p53 signals in the nuclei of nurse cell in the majority of *hemk2*-GLKD ovarioles (Figure 2D; 93%), suggesting that *hemk2*-GLKD resulted in germline cell death in mid-oogenesis. Double-knockdown of *p53* with *hemk2* significantly restored the progression of oogenesis in the *hemk2*-GLKD ovaries (Figure S2B). In addition, the expression of p35, an inhibitor of executioner caspases DrICE and Dcp-1 (Fuchs and Steller, 2015; Werz et al., 2005) also suppressed the cell death in *hemk2*-GLKD ovaries (Figure S2B). Although the females with p53-knocking down or the ectopic expression of p35 in *hemk2*-GLKD females did not fully restore the egg laying as many as the control, the hatching rates of these eggs were comparable to that of the control (Figure S2C). Altogether, we conclude that p53-dependent apoptosis takes place during the mid-oogenesis in *hemk2*-GLKD although the trigger mechanism remains elucidate. However, the chromosomes remained undispersed in *hemk2*-GLKD ovaries restored by the repression of cell death (Figure S2B), suggesting that apoptosis and chromosomal dispersion defects involve distinct pathways triggered by *hemK2* downregulation.

hemK2 **functions for eRF1 methylation and the catalytic activity is essential for oogenesis**

Previous studies reported HemK2 functioned as methyltransferase for three substrates, DNA N6-adenine (6mA) in human culture cells (Xiao et al., 2018), histone H4 lysine 12 (H4K12) in A549 lung adenocarcinoma cells (Metzger et al., 2019) and a glutamine residue in GGQ motif of eRF1 in yeast (Heurgué-Hamard et al., 2005) and human (Figaro et al., 2008). However, its genuine substrate and function in animals remains elusive. Firstly, we examined 6mA modification of genomic DNA upon *hemk2*-GLKD by immunostaining with an anti-6mA antibody. The pattern and the signal intensity of 6mA staining remained unaffected in the germline of *hemk2*-GLKD ovaries (Figure S3A), demonstrating that HemK2 was unlikely to function as methyltransferase for genomic N6-adenine in *Drosophila* germline. In addition, the amount of methylated H4K12 was comparable in *hemk2*-GLKD and the control ovaries (Figure S3B), excluding H4K12 as a bona fide substrate in *Drosophila* germline. Lastly, we examined methylation level of endogenous eRF1 in *hemk2*-GLKD ovaries. Because antibody against methyl-eRF1 did not work for Western blotting, we conducted eRF1 immunoprecipitation followed by immunoblotting with an antibody against N5-methyl-glutamine (Methyl-Q). The methylation level of eRF1 in *hemk2*-GLKD ovaries was considerably reduced to 35% of that of the control, which was possibly due to the unaffected somatic contribution (Figure 3A). Indeed, immunostaining of *hemk2*-GLKD

ovary with anti-methyl-eRF1 antibody revealed a dramatic reduction of eRF1 methylation in germline cells but not in the somatic follicle cells, while the expression level of endogenous eRF1 was comparable in both cell types (Figure 3B). Consistently, immunoprecipitation of germline-expressed FLAG-tagged eRF1 had a scanty of methylation in *hemk2*-GLKD ovaries compared to that of the control (Figure 3C), indicating that *Drosophila* HemK2 mediated methylation of eRF1 at glutamine residue(s). It has been reported that a glutamine residue of a GGQ tripeptide motif in eRF1, which functions for peptide release, is a well-conserved methylation site by HemK2 in other organisms (Dinçbas-Renqvist et al., 2000; Figaro et al., 2008; Gao et al., 2020; Kusevic et al., 2016; Svidritskiy and Korostelev, 2018). We also examined if GGQ tripeptide motif of eRF1 was the methylation target site in S2 cells by mutating the corresponding Gln at 185th position of *Drosophila* eRF1 to Ala (eRF1 Q185A) (Figure 3D). In agreement with those reported in other systems, methylation of eRF1 Q185A was hardly detected in S2 cells even without HemK2 knockdown, suggesting that this mutation perturbed the methylation of eRF1 (Figure 3D). Taken together, these results suggest that Q185 is a predominant methylation site in eRF1 by HemK2.

The rescue experiments described above confirmed that HemK2 had an essential function *in vivo* for the egg development (Figure 1 and Figure S1). We then examined the importance of amino acid residues required for HemK2's catalytic activity during oogenesis in vivo. The highly conserved

NPPY motif of HemK2 is known as a binding pocket of the substrate and essential for the methylation activity of HemK2 in human cell lines (Figure 4A) (Gao et al., 2020; Metzger et al., 2019). Previous study also showed mutations in the relatively-close residues to the substrates, Asn122 and Tyr125, in NPPY motif of human HemK2 disrupted its catalytic activity for methylation of eRF1 *in vitro* (Figure 4B) (Metzger et al., 2019). We mutated the corresponding residues of *Drosophila* HemK2, 116th Asn and 119th Tyr, to alanine (N116A and Y119A, respectively), and expressed them in germline of *hemk2*-GLKD ovaries (Figure 4C; Figure S4A). While HemK2 Y119A did not rescue the defects of *hemK2*-GLKD, such as degeneration of egg chambers, egg laying and hatching rate, HemK2 N116A was able to recover them comparably to those in the control (Figure 4C, D). These results suggest that Tyr119, but not Asn116, was essential for HemK2 function in *Drosophila* germline cells.

Next, we investigated the catalytic activity of HemK2 for methylation of Gln in the GGQ motif of eRF1 in S2 cells. Each FLAG-tagged HemK2 variant and Myc-tagged eRF1 were co-transfected into S2 cells upon knockdown of endogenous *hemk2* (Figure 4E). The immunoprecipitation of Myc-eRF1 followed by immunoblotting with anti-Methyl-Q antibody revealed that methylation of eRF1 was significantly reduced upon *hemk2* knockdown, and such a reduction was successfully rescued by the expression of wildtype HemK2 as well as N116A mutant, but not Y119A (Figure 4E). These results indicate that 119th Tyr but not 116th Asn of *Drosophila* HemK2 is indispensable

to mediate the methylation of eRF1 at 185th Gln.

Several studies previously reported that HemK1, a paralog of HemK2 containing a conserved NPPY motif and 42% homology to HemK2, catalyzed the methylation of Gln in GGQ motif of mitochondrial release factors in human cells (Fang et al., 2022; Ishizawa et al., 2008). To address the specificity of cytosolic eRF1 methylation by HemK2, we examined eRF1 methylation in S2 cells by expression of HemK1 upon *hemk2* knockdown. The reduction of eRF1 methylation by *hemk2* knockdown was successfully rescued by the expression of HemK2 but not by that of HemK1, indicating that eRF1 methylation is uniquely catalyzed by HemK2 (Figure S4B).

eRF1 methylation ensures proper progression of oogenesis and efficient translation

Next, we examined the necessity of eRF1 methylation during oogenesis by knockdown of eRF1's expression in germline cells. Upon *eRF1*-GLKD, ovaries became rudimentary and produced no eggs, showing a severer defect than that of *hemk2*-GLKD ovaries (Figure 5A, B). Immunostaining of eRF1-GLKD ovaries with a germline marker, a DEAD box RNA helicase, Vas, further revealed agametic germaria containing very few germline cells (Figure 5C). Those defects by eRF1-GLKD were successfully rescued with the expression of FLAG-tagged wildtype eRF1 in germline cells but not with that of the methylation-deficient Q185A mutant (Figure 5B, C). These results suggest

that the 185th Gln position, and potentially its methylation, plays a vital role in the survival of germline cells and progression of oogenesis. The milder phenotype observed in *hemk2*-GLKD might have been resulted from the incomplete perturbation of eRF1 methylation, possibly due to residual *hemk2* expression escaped from knockdown or any other enzyme(s) catalyzing eRF1 methylation.

In addition, the expression of FLAG-eRF1 Q185A in the germline cells of the wildtype ovaries resulted in failure in egg production (Figure 5D). Even in the presence of wildtype eRF1, the expression of eRF1 Q185A caused severe developmental arrest at mid-oogenesis as well as failure in chromosome dispersion and massive apoptosis, resembling the defect of *hemk2*-GLKD (Figure 5D; Figure S5A, B). More than 80% of ovarioles expressing eRF1 Q185A contained p53-positive egg chambers (Figure S5C). Taken together, these results suggest that the expression of eRF1 Q185A phenocopies *hemk2*-GLKD; the loss of eRF1 methylation is the main reason causing defects in *hemk2*-GLKD.

It has been reported that the methylation of a Gln residue in eRF1 GGQ motif leads to the release of the nascent polypeptide and assures efficient translational termination (Dinçbas-Renqvist et al., 2000; Figaro et al., 2008; Heurgué-Hamard et al., 2002; Svidritskiy and Korostelev, 2018), and perturbation of proper termination could potentially result in deficient translational activity by inhibiting ribosome recycling. To assess the translation

activity in *hemk2*-GLKD ovaries, we performed an HPG (L-homopropargylglycine) incorporation assay ex vivo with the dissected ovaries. HPG is a methionine analog containing an alkyne moiety and can be ligated to the fluorescent dye through a 'Click reaction' in the presence of copper (II) sulfate (Shen et al., 2021). The fluorescent HPG signal representing the newly synthesized proteins within 30 min in cytoplasm of germline cells was remarkably reduced in *hemk2*-GLKD ovaries (Figure 5E), suggesting that eRF1 methylation was required for efficient translation. Consistent with the capability of eRF1 methylation in S2 cells and of rescuing the defects in *hemk2*-GLKD ovaries (Figure 4C, D, E), the reduction of translation efficiency by *hemk2*-GLKD was fully rescued by the expression of the wildtype *hemk2* as well as N116A mutant but not the Y119A mutant (Figure 5E). In addition, similar to that in *hemK2*-GLKD, the expression of methylation-deficient eRF1 Q185A in germline cells abolished the translation activity (Figure S5D). Altogether, these results suggest that eRF1 methylation by HemK2 is required for the efficient translation activity in *Drosophila* ovary.

***hemk2*-GLKD induced mRNA destabilization via No-Go Decay pathway**

To understand the molecular defects that caused by *hemk2*-GLKD and malfunction of eRF1, we performed the ovarian mRNA-seq analysis by next generation sequencing. The late egg chambers in the control ovaries were cut out to minimize the developmental difference between *hemk2*-GLKD and control ovaries. Consistent with the RT-PCR results described above (Figure

1C and Figure 2C), the reductions of *hemk2* (log2FC=-1.27) and *otu* (log2FC=-1.45) were severely downregulated in the mRNA-seq (Table S4). In addition, 478 upregulated and 325 downregulated genes were detected (log2FC < -1 or >1; q-val < 0.01). GO term analysis (Thomas et al., 2022) of these differentially-expressed genes revealed that *hemk2*-GLKD resulted in severe downregulation of many genes involved in the female reproductive processes, such as female gamete generation, oogenesis and germ cell development (Figure 6A). In contrast, genes involved in processes unrelated to oogenesis were relatively upregulated (Figure 6B). To further examine the impact of gene expression upon germline-knockdown of *hemk2*, we took advantage of previous study reporting gene expression in different ovarian cell types based on the single cell mRNA analysis; two germline and somatic cell types were identified by the gene expression patterns. Among those, we focused on genes expressed in 1 germline and 5 somatic cell types, the represented cell types in early to mid-oogenesis to see the changes of mRNA abundance. Of note, genes enriched in Germline 2 cell type (N=154), which are expressed from region 2 onward, were most downregulated (average log2FC = -0.55) in *hemk2*-GLKD versus control (Figure 6C) (Jevitt et al., 2020). In contrast, the expression of genes enriched in 5 different somatic-cell types did not show any significant change (Figure 6D; Figure S6A-E). These results suggest that perturbation of eRF1 function in germline cells by *hemk2*-knockdown specially downregulates mRNAs.

Previous studies have demonstrated that methylation of eRF1 at GGQ motif enhances the release of nascent peptide and increases the rate of translation termination by 10 to 100 times (Pierson et al., 2016). Thus, we hypothesized that perturbation of the methylation on eRF1 reduced the release rate of the nascent peptides, leading to the ribosome stalling at the stop codons on the actively translated mRNAs. Such ribosome stalling is known to trigger Ribosome-associated Quality Control (RQC), eliminating mRNAs being actively translated with bound ribosomes in a process called no-go decay (NGD) (Brandman and Hegde, 2016; Doma and Parker, 2006; Ikeuchi et al., 2019; Simms et al., 2017; Tomomatsu et al., 2023). To address this possibility, first, we investigated the ribosome stalling in *hemk2*-GLKD. We conducted sucrose gradient sedimentation assay using *hemk2*-GLKD ovarian lysate to examine whether ribosomes are collided by inefficient translation termination. Ribosomes in the ovarian lysate were fixed with a translation inhibitor, emetine, incubated with RNase to cleave the unprotected region of mRNA, and analyzed through the sucrose gradient. The monosome was a major population and a disome caused by a ribosome collision was hardly detected in the control (Figure 6E). Upon *hemk2*-GLKD, however, the ratio of disome significantly increased (Figure 6E, h*emk2*-GLKD), suggesting that the inefficient release of the nascent polypeptide caused by unmethylated eRF1 resulted in the ribosome collision.

Next, we examined whether NGD contributed to severe defects observed

in *hemk2*-GLKD. To address this possibility, NGD pathway was simultaneously knocked down together with *hemk2* in germline cells and the defects were investigated (Figure 7 and Figure S7A). In the double-germline knockdown (DGKD) ovaries of *hemk2* and *ski8*, a component of the Ski complex which threads mRNAs into the exosome and promotes 3' to 5' degradation (Anderson and Parker, 1998), the developmental defects in *hemk2*-GLKD were partially rescued (Figure 7A). *ski8-hemk2* DGKD females contained later stages of egg chambers and laid the comparable number of eggs, albeit the hatching rate remained 40% of the control (Figure 7A, B). Because the Ski complex is rather a component involved in general RNA degradation, we further examined other factors which specifically function for NGD, such as *pelota* (*pelo*), a critical effector of NGD pathway which functions for dissociation of stalled ribosomes and RNA degradation (Becker et al., 2011; Jamar et al., 2017; Kobayashi et al., 2010; Tsuboi et al., 2012). Intriguingly, similar to *ski8-hemk2* DGKD, *pelo-hemk2* DGKD female also possessed later egg chambers and laid the comparable numbers of eggs with 60% hatching rate (Figure7A, B). We also examined another potential NGD component, an endonuclease called *nonu-1*/*cue2* reported in *C. elegans* and *S. cerevisiae* which cleaves mRNAs following the ribosome stalling during translation (D'Orazio et al., 2019; Glover et al., 2020) (Figure S7B). Unlike *ski8* and *pelo*, however, double-germline knockdown of *CG7139*, the *Drosophila* homolog of *nonu-1*/*cue2*, and *hemk2* did not show any restoration of defects caused

(Figure 7A, B; Figure S7A). This suggests that in *Drosophila*, *CG7139* is not essential in NGD pathway, or it may function redundantly with other endonucleases during translation surveillance induced by *hemk2*-GLKD. In addition, double-germline knockdown of *hemk2* and *upf3*, a factor involved in nonsense-mediated decay (NMD) (Tan et al., 2022), did not rescue the defects in *hemk2*-GLKD (Figure 7A, B), proving a specific action of NGD triggering mRNA degradation. We confirmed the effective knocking down of each examined component in ovaries by qRT-PCR (Figure S7A; ranging from 10 to 30 % compared to that of the control); considering the contribution of non-knockdown somatic cell fractions to entire ovarian RNAs, the expression of each factor was significantly reduced. Consistent with their capability to rescue in the developmental morphology of *hemk2*-GLKD, the HPG assay revealed that knockdown of *ski8* or *pelo*, but not *CG7139* or *upf3*, in *hemk2*-GLKD ovaries partly rescued the reduction of translational activity (Figure 7C, D). All together, these data suggest that the perturbation of eRF1 methylation in *hemk2*-GLKD ovaries leads to poor translation termination and ribosome stalling, which triggers mRNA degradation specifically through the NGD pathway.

Consistent with the observed restoration of oogenesis defects in *hemk2*-GLKD ovaries, the expression levels of those downregulated protein-coding RNAs were recovered by the additional germline knockdown of *ski8* or *pelo* (Figure S6F, G), further confirming that NGD was specifically

activated for the mRNA degradation upon *hemk2*-GLKD. Double-germline knockdown of *ski8* or *pelo and hemk2* also restored the overall protein synthesis, although the ribosome stalling was observed to similar extent of that in the *hemk2*-single knockdown (Figure 6E). These results imply that translation re-initiation could take place to synthesize proteins to some extent when mRNAs are not cleared by NGD, partly restoring egg maturation (Figure 7A, B). Overall, these findings indicate that perturbation of eRF1 methylation in *hemk2*-GLKD leads to inefficient release of synthesized peptides, triggering RQC and activation of the NGD pathway, possibly by the ribosome stalling.

Discussion

The knockdown of *hemk2* resulted in female sterility, with a significant disruption in oogenesis development observed in both ovarian germline and somatic cells, leading to a developmental arrest in the mid-stage (Figure 1; Figure S1). Curiously, *hemk2*-GLKD ovaries exhibited the morphological defects, hyperplasia of the posterior follicle cells and failure in chromosomal dispersion (Figure 2A, B). Previous studies reported that Delta ligand expressed in germline cells Notch-Delta signaling triggers, inducing a transition from mitotic cell cycle to endocycle in follicle cells (Deng et al., 2001; Schaeffer et al., 2004; St. Johnston, 2001). The observed hyperplasia of the posterior follicle cells in *hemk2*-GLKD ovaries may be attributed to the downregulation of Delta ligand in germline cells, which in turn results in the prolonged mitotic division of follicle cells even beyond stage 6.

In stage 6 and older egg chambers, almost all *hemk2*-GLKD ovarioles exhibited the presence of undispersed chromosomes within nurse cell nuclei (Figure 2B; Figure S2A). Some of genes involved in RNA regulation, such *otu*, *hfp*, and *smn* were significantly downregulated in *hemk2*-GLKD ovaries (King et al., 1981; Lee et al., 2009; Van Buskirk and Schüpbach, 2002). Similar to that in *hemK2*-GLKD, mutations in these genes also produce defects in nurse cell chromosome dispersal (Goodrich et al., 2004; Klusza and Deng, 2010; Lee et al., 2009; Steinhauer and Kalfayan, 1992). Among those, one of two isoforms coded by *otu* locus, Otu104, is known to function for the chromosome

445 dispersion of nurse cells (Goodrich et al., 2004; Klusza and Deng, 2010; Van
446 Buskirk and Schüpbach, 2002). Consistently, the expression of Otu104 slightly
447 rescued the chromosome dispersion defect observed in *hemk2*-GLKD (Figure
448 S2A). However, egg chambers remained small (Figure S2A), indicating the
449 impact of *hemk2*-GLKD on egg formation was not restored by Otu104
450 expression. Conversely, the repression of cell death in *hemk2*-GLKD ovaries
451 significantly rescued the egg formation in *hemk2*-GLKD ovaries, yet the nurse
452 cell chromosomes remained undispersed (Figure S2B). Collectively, our
453 results suggest that germline cell death in *hemk2*-GLKD is not attributed to the
454 chromosomal dispersion defect but possibly rather to ribosome stalling
455 resulting from the perturbation of eRF1 methylation (Wu et al., 2020). It has
456 been reported that the ribosome collision triggers two distinct stress response
457 pathways; transient collision evokes GCN2-mediated pathway for cell survival,
458 and severer collision activates MAPKK inducing apoptosis in human cell lines
459 (Wu et al., 2020). Our observation suggests that insufficient methylation by
460 *hemk2* knockdown results in ribosome stalling and collision, thereby inducing
461 apoptosis in vivo, the translationally-active *Drosophila* ovaries.

462 Three potential substrates, DNA 6mA, histone H4K12 and eRF1, have
463 been previously identified for HemK2 in yeast and mammalian culture cells
464 (Figaro et al., 2008; Metzger et al., 2019; Xiao et al., 2018). Our study revealed
465 that *hemk2* knockdown did not affect methylation patterns of DNA 6mA or
466 histone H4K12 (Figure S3A, B), but caused a significant decrease in eRF1

methylation levels (Figure 3A-C), demonstrating the substrate specificity of *Drosophila* HemK2 for eRF1. The 119th Tyr but not 116th Asn of *Drosophila* HemK2 was indispensable and critical for its function in oogenesis and eRF1 methylation (Figure 4C-E). These results were discrepant from the fact that both of the corresponding residues in human HemK2 were essential for eRF1 methylation *in vitro* (Metzger et al., 2019). Recent structural studies for human HemK2, however, suggested that the side chain of Asn122 was not involved in binding to methylated glutamine in the substrate biding pocket of HemK2 (Gao et al., 2020), which is consistent with the dispensability of Asn116 for HemK2 methyltransferase activity.

The examination of murine HemK2's substrate specificity through a peptide substrate array revealed a potential consensus motif: G-Q-[SRYKLGAMTC]-[ARFGLWYCSQKH]-[LARCQFYT]-R, where [ ] denotes any one residue among those listed inside (Kusevic et al., 2016). By using this consensus motif, we identified several possible substrates of HemK2 among *Drosophila melanogaster* proteins, such as CG17841, Spargel, Chd1, Ythdc1, and eRF1. These potential substrates may be methylated by HemK2 in particular conditions. However, the overexpression of the methylation-deficient eRF1 Q185A mutant recapitulated the phenotypic characteristics observed in *hemk2*-GLKD (Figure 5D), suggesting that eRF1 serves as the primary substrate for *Drosophila* HemK2 in germline cells.

Previous studies have reported that the methylation of the conserved

GGQ motif in release factors significantly enhances the release of nascent peptide and substantially increased the termination rate of protein synthesis by a magnitude of 10 to 100 times (Pierson et al., 2016). In agreement with this, the translation efficiency was remarkably reduced upon perturbation of eRF1 methylation by *hemk2*-GLKD (Figure 5E). Such a reduction in protein synthesis as well as oogenesis defect and down regulation of mRNAs were significantly restored by the blockade of a general RNA degradation or NGD pathway, but not by NMD (Figure 7A-D). These results suggest that the residual activity of the ribosome along with unmethylated eRF1 can manage to synthesize the minimal amounts of polypeptides when mRNAs are provided for the translation.

Our study provides evidence that HemK2 acts as a genuine protein methyltransferase in *Drosophila* and plays a crucial role in modulating the activity of eRF1 by glutamine methylation, which is indispensable for proper germline development. Germline nurse cells produce large amounts of proteins and mRNAs to transfer them to oocyte. Thus, it is important to regulate the costly protein synthesis. However, the regulation mechanism of eRF1 methylation by HemK2 remains to be fully elucidated and requires further investigation. This mechanism may function to maximize egg formation under favorable physiological conditions but suppress it under unfavorable ones.

Materials and Methods

Fly stocks and cultures

All stocks and crosses were raised at room temperature (RT) or 25°C on standard food (5%(w/v) dry yeast, 5%(w/v) corn flower, 2%(w/v) rice bran, 10%(w/v) glucose, 0.7%(w/v) agar, 0.2%(v/v) propionic acid, 0.05%(v/v) p-hydroxy butyl benzoic acid). For knockdown experiments, the following TRiP lines obtained from Bloomington Drosophila Stock Center (IN, USA) were used in this study: *hemk2* (HMS02003, #40837), *eRF1* (HMS05812, #67900), *upf3* (HMJ22158, #58181), *cue2* (HMS02721, #44007), *ski8* (HMC04664, #57377), *p53* (HMS02286, #41720). attP40 (#25709) and attP2 (#25710) were used for injection. The following drivers were used to express transgenes or shRNAs: *NGT40* and *nosGal4-VP16* (Grieder et al., 2000), *Matα-tub-GAL4* (#7063), and *traffic jam-Gal4* (DGRC# 104055) (Hayashi et al., 2002). UASp-P35 transgenic line was a kind gift from Dr. Bergmann (Werz et al., 2005). Either the *y w* strain or the respective heterozygote was used as a control in each experiment.

Generation of transgenic fly lines

The generated transgenic lines were as follows: FLAG-HemK2 wildtype at P2, FLAG-HemK2 N116A at P2, FLAG-HemK2 Y119A at P2, FLAG-snapin at P2, FLAG-eRF1 wildtype at P2, FLAG-eRF1 Q185A at P2, FLAG-*otu*104 at P2. In each case, the coding sequence or its mutant form was amplified by PCR using *y w* genomic DNA (gDNA) or the cDNAs obtained by reverse

transcription from ovarian RNA of *y w* flies as template, and triple repeats of the FLAG tag were added to the N-terminal region. Purified PCR fragments were cloned into the *Xba*I-linearized pUASp-K10-attB vector (Koch et al., 2009) by In-Fusion reaction (#639648, Takara Bio, Japan). The positive plasmids were injected into embryo of nos-phiC31;;P{CaryP} attP2 (#25710) by using the standard protocol.

hemk2 TRiP at P2, and *pelo* TRiP at P2 and P40 were generated in this study. TRiP constructs were generated by introducing the annealed oligos (TRiP-Fw/Rv) into *Nhe*I- and *Eco*RI-linearized pWalium22 vector (Perkins et al., 2015) by DNA ligation. The UASp and Walium22 plasmids were then injected into embryo of nos-phiC31; P{CaryP}attP40 (#25709) or nos-phiC31;;P{CaryP} attP2 (#25710). The oligos used for annealing are listed in Table S1.

Fluorescent immunostaining

Immunostaining was performed as previously reported (Lim et al., 2022). Ovaries were dissected and teased apart slightly in phosphate-buffered saline (PBS), followed by fixation with 5.3% (v/v) paraformaldehyde (PFA, Electron Microscopy Sciences, United States) in PBS for 10 min at RT. Fixed ovaries were washed for 30 min with several changes of PBX (PBS containing 0.2% (v/v) Triton X-100), and incubated with PBX containing 4% (w/v) bovine serum albumin (BSA) for at least 30 min of blocking. The incubation with primary

553 antibodies in PBX containing 0.4% (w/v) BSA was performed overnight at 4°C,
554 and ovaries were washed for 1 h with several changes of PBX. The secondary
555 antibody incubation was then conducted for >2 h at room temperature, and
556 ovaries were washed for 1 h with PBX and stained with 1 μg/ml of
557 4′6-diamidine-2′-phenylindole (DAPI) (SIGMA, United States) for 10 min in
558 PBX. After rinsing with PBS, the ovaries were mounted with Fluoro-KEEPER
559 Antifade (Nacalai Tesque, Japan) onto a slide.

560 The following primary antibodies were used in the indicated dilution;
561 mouse anti-FLAG (SIGMA [M2], Cat.# F1804, 1:200), guinea pig anti-Vas
562 (1:2,000) (Patil and Kai, 2010), rabbit anti-pH3 (Millipore, Cat.# 06-570, 1:250),
563 mouse anti-p53 (DSHB [25F4], 1:100), rabbit anti-Fibrillarin (Abcam, Cat.#
564 ab5821, 1:200), rabbit anti-DNA 6mA (pAbmAbs, Cat.# 202003, 1:1,000),
565 rabbit anti-eRF1 (SIGMA, Cat.# E8156, 1:200), rabbit anti-methyl-eRF1 (1:100)
566 (Lacoux et al., 2020). The following secondary antibodies were used in this
567 study; Alexa Fluor 488-, 555- conjugated goat antibodies against rabbit,
568 mouse, and guinea pig IgG (Invitrogen, Cat.#: A11029, A11034, A11073,
569 A21424, A21429, A21435) were used at 1:200 in PBX containing 0.4% (w/v)
570 BSA. Images of the ovaries were taken by Zeiss LSM 900 confocal
571 microscope and processed using Zen (Zeiss) and Fiji (Schindelin et al., 2012)
572 software.

573 **Protein synthesis assay**

The Click-iT® HPG Alexa Fluor 488 Protein Synthesis Assay kit (Molecular probes, United States) was used to monitor newly synthesized proteins by quantification of fluorescent HPG signals. The freshly dissected ovaries were treated with 1 mM HPG in PBS for 30 min and fixed in 5.3% PFA in PBS for 10 min. Subsequently, the ovaries were permeabilized with PBX for 30 min by washing three times (3% BSA/PBX for the first time, PBX only for the second and third time). They were then incubated with a freshly prepared Click-iT® reaction cocktail for 30 min. After washing with Click-iT® reaction rinse buffer, the ovaries were incubated with HCS NuclearMask™ Blue Stain working solution (1:2,000 in PBX) for 30 min according to manufacturer's protocol. The samples were further immunostained with antibodies, and the images were taken as described above.

Quantification analysis of HPG signal for translation activity

Each image was processed with Fiji software. The fluorescence intensity of HPG signals in the cytosolic (non-nucleus) regions of nurse cells was measured. Each small square (in identical size) was calculated after background (blank area without any imaging) subtraction, and 2-5 squares per egg chamber (stage 3-8) were analyzed. The mean value of all squares per image was quantified as translation activity and 5 images were quantified per genotype.

Immunoprecipitation and Western blotting

One hundred ovaries were dissected in cold PBS and homogenized with a pestle in PBST (PBS with 0.1%(v/v) Tween-20) supplemented with proteinase inhibitor cocktail (PIC, #11873580001, Roche, Switzerland). After centrifugation at 15,000 xg for 10 min at 4°C, supernatant was collected, 10 µl of Protein G magnetic beads (TAMAGAWA SEIKI, #TAS8848N1173) was incubated with FLAG antibody (SIGMA [M2], Cat.# F1804) or (5 µl beads for eRF1 case) for more than 1 h at 4°C with gentle rotation before adding lysate. Subsequently the antibody-conjugated beads were washed twice with cold PBST and incubated with lysate at 4°C for 3-4 h. Proteins were rinsed with cold PBST three times and eluted from beads in 50 µl of sample buffer at 95°C for 5 min.

Protein lysates or immunoprecipitates were separated by SDS-PAGE and transferred to a 0.45 µm Clear Trans® PVDF membrane (Wako, Japan). The membrane was blocked in PBST with 3% (w/v) skim milk (Nacalai Tesque, Japan) and incubated with the following primary antibodies diluted in the signal enhancer reagent HIKARI (Nacalai Tesque): rabbit anti-eRF1 (SIGMA, Cat.# E8156, 1:1,000), rabbit anti-Methyl-Q (Millipore, Cat.# ABS2185, 1:1000), mouse anti-FLAG (SIGMA [M2], Cat.# F1804, 1:1,000), mouse anti-c-Myc (Wako [9E10], Cat.# 017-21871, 1:1,000), mouse anti-histone H4 (MAB Institute, Cat.# 388-09171, 1:2000), rabbit anti-H4K12met (PTM BIO, Cat.# PTM-685RM, 1:2,000), mouse anti-Tubulin (Santa Cruz [DM1A], Cat.# sc-32293, 1:3,000), rabbit anti-HA (Cell signaling Technology [C29F4], Cat.#

3724, 1:1,000).

HRP-conjugated secondary antibodies used in this study were as follows: goat anti-rabbit IgG, or anti-mouse IgG (1:3,000; #170-6515, #170-6516, Bio-Rad, CA, United States). To avoid signals from IgG heavy chain overlapping with eRF1, VeriBlot-HRP (Abcam, #ab131366, 1:1,000) was used in Western blot analysis for immunoprecipitation of endogenous eRF1 or FLAG-eRF1. Chemi-Lumi One (Nacalai Tesque, #07880-70) was used to obtain the chemiluminescent signals, which were then imaged by ChemiDoc™ Touch MP (Bio-Rad). Band intensities were quantified from independent experiments by Image Lab software (Bio-Rad).

Quantitative RT-PCR

Total RNAs were extracted from ovaries using TRIzol LS (Invitrogen) in strict accordance with the manufacturer's instructions. Following this, the purified RNA (1 μg) was subjected to DNase I treatment (Invitrogen) to eliminate any genomic contamination, which was subsequently inactivated using EDTA. cDNAs were synthesized by reverse transcription with Superscript III system (Invitrogen) following the manufacturer's protocol. The qPCR experiment was carried out using KAPA SYBR Fast qPCR Master Mix (KAPA biosystems) in the StepOnePlus Real-Time PCR system (Applied Biosystems). The relative expression levels were normalized to those of *rp49* with three biological replicates and technical duplicates. The primer sequences

for detecting the expression levels of genes are shown in Table S2.

S2 cell experiments

Drosophila S2 cells were cultured at 28°C in Schneider medium containing 10% (v/v) Fetal Bovine Serum (FBS), supplemented with penicillin and streptomycin. The endogenous *hemk2* was knocked down by dsRNA targeting a 186bp region starting from ATG codon of *snapin* gene (Figure S1). The dsRNA was generated by *in vitro* AmpliScribe T7 High Yield transcription kit (Lucigen, United States). The primers used for PCR are listed in Table S3.

Plasmids used for transfection were as follows: Myc-HemK2 wildtype, Myc-HemK2 N116A, Myc-HemK2 Y119A, FLAG-eRF1 wildtype, FLAG-eRF1 Q185A, Myc-HemK1. The constructions were generated using the Gateway system (Life technologies) and transfected by HilyMax (Dojindo Molecular Technologies, Inc, Japan) following the manufacturer's instructions. The immunoprecipitation and immunoblotting were conducted as described above.

Fertility test

To test female fertility, *y w* males were mated with three eclosed females of each genotype for few days in vials with normal food, and then transferred to apple juice plates with a bit of wet yeast paste. The total number of eggs laid by mated females was counted, and the unhatched eggs were quantified to determine the hatching rates after 24 hours of egg laying. To analyze the fertility of *hemk2*-GLKD males, three *y w* virgin females were mated with

hemk2-GLKD males for longer time, and the following statistics were recorded. Each experiment was conducted in three biological replicates.

mRNA-seq analyses

Total RNAs of each genotype in two biological replicates were extracted from dissected ovaries using TRIzol LS (Invitrogen) in accordance with the manufacturer's protocol. Because *hemk2* knockdown ovaries did not contain later stages, regions later than mid oogenesis were eliminated by cutting the ovaries for RNA preparation to minimize the developmental stage difference. Poly(A)-tailed RNAs were isolated and concentrated using oligo-dT beads in NEBNext® Poly(A) mRNA Magnetic Isolation Module (New England Biolabs, USA), subsequently subjected to fragmentation and reverse transcription. After ligation of adapters, PCR amplification was performed to generate the libraries (NEBNext® UltraTM II Directional RNA Library Prep Kit, New England Biolabs, USA). The cDNA library preparation and next-generation sequencing were performed by Rhelixa Inc (Japan). Around 13 million paired sequences were obtained for each sample. Reads with low quality and adapter sequences were removed by fastp program (Chen et al., 2018). Subsequently, reads were mapped on the *Drosophila* melanogaster genome reference (dm6) by STAR program (Dobin et al., 2013). The counts of the mapped reads for genes were analyzed by featureCounts (Liao et al., 2014). The statistical analysis for the differential expression genes were performed using DESeq2 (Love et al., 2014). The upregulated genes (log2FoldChnage > 1, p-adj < 0.01)) and

downregulated genes (log2FoldChange < -1, p-adj < 0.01) were selected and subjected to the GO term overrepresentation analysis by PANTHER (Thomas et al., 2022).

Monosome/Disome profiling

Ovaries were dissected in polysome lysis buffer (20 mM Tris-Cl, pH 7.5, 5 mM $MgCl_2$, 100 mM NaCl) supplemented with 0.1% NP-40, 200 µg/ml emetine (E2375, SIGMA), and PIC. The dissected ovaries were snap frozen in liquid nitrogen and stored at -80ºC with minimum volume of the buffer. Around 30 pairs of ovaries were homogenized with plastic pestle in 500 µl of polysome lysis buffer supplemented with 0.1% CHAPS (Nacalai Tesque, Japan), 200 µg/ml emetine, and PIC. The lysate was centrifuged at 15,000 xg for 5 min at 4ºC. Supernatant was further centrifuged at 15,000 xg for 15 min at 4ºC and 250 µl of the supernatant was collected. The RNA concentration in the supernatant was determined by Qubit RNA HS assay kit (Q32852, Invitrogen). The RNA concentration in the supernatant was adjusted to 0.05 µg/µl by adding polysome lysis buffer supplemented with 0.1% CHAPS, 200 µg/ml emetine, and PIC. The resulted lysate was incubated with RNase A (1 µg/ml) for 10 min at 25ºC to cleave the unprotected region of RNA. 200 µl of the RNase A-treated sample was loaded on the top of the sucrose gradient (10%-50% sucrose in polysome lysis buffer) in SW41Ti and centrifuged at 30,000 xg for 3 h at 4ºC. After centrifugation, the gradients were fractionated from the top using piston gradient fractionator (BioComp, Canada).

703

Acknowledgments

We thank Dr Valérie Heurgué-Hamard (IBPC, Paris) for a generous gift of antibody against methyl-eRF1. We acknowledge Bloomington Drosophila Stock Centre and Kyoto Stock Center for the fly stocks. Assistance with sucrose gradient analysis was provided by the Center for Medical Research and Education, Graduate School of Medicine, Osaka University. We appreciate the insightful discussion and suggestions from all the members of KT's laboratory.

Author Contributions

All authors contributed to the experiment design. XF, SR, KS, and KT performed all experiments. XF, SR and KS performed the computational analyses. XF, SR, KS, and KT wrote the paper. KS, IT, and KT supervised the project.

Funding Statement

This work was supported by TAKEDA Bioscience Research Grant (J191503009) for KT, Grant-in-Aid for Scientific Research on Innovative Areas (20H05390) for KT, Grant-in-Aid for Transformative Research Areas (A) (21H05275) for KT, and Osaka University Institute for Datability Science "Transdisciplinary Research Project" (Na22990007) for KT and KS.

Data And Material Availability

NGS data sets have been deposited to the DNA Data Bank of Japan (DDBJ). BioProject Accession: PRJDB17326. All fly strains generated for this study are available upon request.

Conflict Of Interest Statement

The authors declare that the research was conducted in the absence of any commercial or financial relationships that could be construed as a potential conflict of interest.

References

Anderson, J.S., Parker, R.P., 1998. The 3' to 5' degradation of yeast mRNAs is a general mechanism for mRNA turnover that requires the SKI2 DEVH box protein and 3' to 5' exonucleases of the exosome complex. EMBO J. 17, 1497–1506. https://doi.org/10.1093/emboj/17.5.1497

Avilés-Pagán, E.E., Orr-Weaver, T.L., 2018. Activating embryonic development in Drosophila. Semin. Cell Dev. Biol. 84, 100–110. https://doi.org/10.1016/j.semcdb.2018.02.019

Becker, T., Armache, J.-P., Jarasch, A., Anger, A.M., Villa, E., Sieber, H., Motaal, B.A., Mielke, T., Berninghausen, O., Beckmann, R., 2011. Structure of the no-go mRNA decay complex Dom34–Hbs1 bound to a stalled 80S ribosome. Nat. Struct. Mol. Biol. 18, 715–720. https://doi.org/10.1038/nsmb.2057

Brandman, O., Hegde, R.S., 2016. Ribosome-associated protein quality control. Nat. Struct. Mol. Biol. 23, 7–15. https://doi.org/10.1038/nsmb.3147

Chen, C.-C., Wang, K.-Y., Shen, C.-K.J., 2013. DNA 5-methylcytosine demethylation activities of the mammalian DNA methyltransferases. J. Biol. Chem. 288, 9084–9091. https://doi.org/10.1074/jbc.M112.445585

Chen, S., Zhou, Y., Chen, Y., Gu, J., 2018. fastp: an ultra-fast all-in-one FASTQ preprocessor. Bioinformatics 34, i884–i890. https://doi.org/10.1093/bioinformatics/bty560

Clarke, S.G., 2013. Protein methylation at the surface and buried deep: thinking outside the histone box. Trends Biochem. Sci. 38, 243–252. https://doi.org/10.1016/j.tibs.2013.02.004

Dai, X., Ren, T., Zhang, Y., Nan, N., 2021. Methylation multiplicity and its clinical values in cancer. Expert Rev. Mol. Med. 23, e2. https://doi.org/10.1017/erm.2021.4

Dej, K.J., Spradling, A.C., 1999. The endocycle controls nurse cell polytene chromosome structure during *Drosophila* oogenesis. Development 126, 293–303. https://doi.org/10.1242/dev.126.2.293

Deng, W.-M., Althauser, C., Ruohola-Baker, H., 2001. Notch-Delta signaling induces a transition from mitotic cell cycle to endocycle in *Drosophila* follicle cells. Development 128, 4737–4746. https://doi.org/10.1242/dev.128.23.4737

Dinçbas-Renqvist, V., Engström, Å., Mora, L., Heurgué-Hamard, V., Buckingham, R., Ehrenberg, M., 2000. A post-translational modification in the GGQ motif of RF2 from Escherichia coli stimulates termination of translation. EMBO J. 19, 6900–6907. https://doi.org/10.1093/emboj/19.24.6900

Dobin, A., Davis, C.A., Schlesinger, F., Drenkow, J., Zaleski, C., Jha, S., Batut, P., Chaisson, M., Gingeras, T.R., 2013. STAR: ultrafast universal RNA-seq aligner. Bioinformatics 29, 15–21. https://doi.org/10.1093/bioinformatics/bts635

Doma, M.K., Parker, R., 2006. Endonucleolytic cleavage of eukaryotic mRNAs with stalls in translation elongation. Nature 440, 561–564. https://doi.org/10.1038/nature04530

D'Orazio, K.N., Wu, C.C.-C., Sinha, N., Loll-Krippleber, R., Brown, G.W., Green, R., 2019. The endonuclease Cue2 cleaves mRNAs at stalled ribosomes during No Go Decay. eLife 8, e49117.

https://doi.org/10.7554/eLife.49117

Drummond-Barbosa, D., Spradling, A.C., 2001. Stem Cells and Their Progeny Respond to Nutritional Changes during Drosophila Oogenesis. Dev. Biol. 231, 265–278. https://doi.org/10.1006/dbio.2000.0135

Fang, Q., Kimura, Y., Shimazu, T., Suzuki, T., Yamada, A., Dohmae, N., Iwasaki, S., Shinkai, Y., 2022. Mammalian HEMK1 methylates glutamine residue of the GGQ motif of mitochondrial release factors. Sci. Rep. 12, 4104. https://doi.org/10.1038/s41598-022-08061-y

Figaro, S., Scrima, N., Buckingham, R.H., Heurgué-Hamard, V., 2008. HemK2 protein, encoded on human chromosome 21, methylates translation termination factor eRF1. FEBS Lett. 582, 2352–2356. https://doi.org/10.1016/j.febslet.2008.05.045

Fuchs, Y., Steller, H., 2015. Live to die another way: modes of programmed cell death and the signals emanating from dying cells. Nat. Rev. Mol. Cell Biol. 16, 329–344. https://doi.org/10.1038/nrm3999

Gao, J., Wang, B., Yu, H., Wu, G., Wan, C., Liu, W., Liao, S., Cheng, L., Zhu, Z., 2020. Structural insight into HEMK2–TRMT112-mediated glutamine methylation. Biochem. J. 477, 3833–3838. https://doi.org/10.1042/BCJ20200594

Gates, L.A., Foulds, C.E., O'Malley, B.W., 2017. Histone Marks in the 'Driver's Seat': Functional Roles in Steering the Transcription Cycle. Trends Biochem. Sci. 42, 977–989. https://doi.org/10.1016/j.tibs.2017.10.004

Gleason, R.J., Anand, A., Kai, T., Chen, X., 2018. Protecting and Diversifying the Germline. Genetics 208, 435–471. https://doi.org/10.1534/genetics.117.300208

Glover, M.L., Burroughs, A.Max., Monem, P.C., Egelhofer, T.A., Pule, M.N., Aravind, L., Arribere, J.A., 2020. NONU-1 Encodes a Conserved Endonuclease Required for mRNA Translation Surveillance. Cell Rep. 30, 4321-4331.e4. https://doi.org/10.1016/j.celrep.2020.03.023

Goodrich, J.S., Clouse, K.N., Schüpbach, T., 2004. Hrb27C, Sqd and Otu cooperatively regulate *gurken* RNA localization and mediate nurse cell chromosome dispersion in *Drosophila* oogenesis. Development 131, 1949–1958. https://doi.org/10.1242/dev.01078

Grieder, N.C., Cuevas, M.D., Spradling, A.C., 2000. The fusome organizes the microtubule network during oocyte differentiation in *Drosophila*. Development 127, 4253–4264. https://doi.org/10.1242/dev.127.19.4253

Hayashi, S., Ito, K., Sado, Y., Taniguchi, M., Akimoto, A., Takeuchi, H., Aigaki, T., Matsuzaki, F., Nakagoshi, H., Tanimura, T., Ueda, R., Uemura, T., Yoshihara, M., Goto, S., 2002. GETDB, a database compiling expression patterns and molecular locations of a collection of gal4 enhancer traps. genesis 34, 58–61. https://doi.org/10.1002/gene.10137

Heurgué-Hamard, V., Champ, S., Engström, A., Ehrenberg, M., Buckingham, R.H., 2002. The hemK gene in Escherichia coli encodes the N(5)-glutamine methyltransferase that modifies peptide release factors. EMBO J. 21, 769–778. https://doi.org/10.1093/emboj/21.4.769

Heurgué-Hamard, V., Champ, S., Mora, L., Merkoulova-Rainon, T., Kisselev, L.L., Buckingham, R.H., 2005. The Glutamine Residue of the Conserved GGQ Motif in Saccharomyces cerevisiae Release Factor eRF1 Is Methylated by the Product of the YDR140w Gene *. J. Biol. Chem. 280, 2439–2445. https://doi.org/10.1074/jbc.M407252200

Heurgué-Hamard, V., Graille, M., Scrima, N., Ulryck, N., Champ, S., van Tilbeurgh, H., Buckingham, R.H., 2006. The zinc finger protein Ynr046w is plurifunctional and a component of the eRF1 methyltransferase in yeast. J. Biol. Chem. 281, 36140–36148. https://doi.org/10.1074/jbc.M608571200

Ikeuchi, K., Izawa, T., Inada, T., 2019. Recent Progress on the Molecular Mechanism of Quality Controls Induced by Ribosome Stalling. Front. Genet. 9, 743. https://doi.org/10.3389/fgene.2018.00743

Ishizawa, T., Nozaki, Y., Ueda, T., Takeuchi, N., 2008. The human mitochondrial translation release factor HMRF1L is methylated in the GGQ motif by the methyltransferase HMPrmC. Biochem. Biophys. Res. Commun. 373, 99–103. https://doi.org/10.1016/j.bbrc.2008.05.176

Jamar, N.H., Kritsiligkou, P., Grant, C.M., 2017. The non-stop decay mRNA surveillance pathway is required for oxidative stress tolerance. Nucleic Acids Res. 45, 6881–6893. https://doi.org/10.1093/nar/gkx306

Jevitt, A., Chatterjee, D., Xie, G., Wang, X.-F., Otwell, T., Huang, Y.-C., Deng, W.-M., 2020. A single-cell atlas of adult Drosophila ovary identifies transcriptional programs and somatic cell lineage regulating oogenesis. PLOS Biol. 18, e3000538. https://doi.org/10.1371/journal.pbio.3000538

King, R.C., Riley, S.F., Cassidy, J.D., White, P.E., Paik, Y.K., 1981. Giant Polytene Chromosomes from the Ovaries of a Drosophila Mutant. Science 212, 441–443. https://doi.org/10.1126/science.6782674

Klotz, A.V., Thomas, B.A., Glazer, A.N., Blacher, R.W., 1990. Detection of methylated asparagine and glutamine residues in polypeptides. Anal. Biochem. 186, 95–100. https://doi.org/10.1016/0003-2697(90)90579-X

Klusza, S., Deng, W.-M., 2010. poly is required for nurse-cell chromosome dispersal and oocyte polarity in Drosophila. Fly (Austin) 4, 128–136.

Klusza, S., Novak, A., Figueroa, S., Palmer, W., Deng, W.-M., 2013. Prp22 and Spliceosome Components Regulate Chromatin Dynamics in Germ-Line Polyploid Cells. PLoS ONE 8, e79048. https://doi.org/10.1371/journal.pone.0079048

Kobayashi, K., Kikuno, I., Kuroha, K., Saito, K., Ito, K., Ishitani, R., Inada, T., Nureki, O., 2010. Structural basis for mRNA surveillance by archaeal Pelota and GTP-bound EF1α complex. Proc. Natl. Acad. Sci. U. S. A. 107, 17575–17579. https://doi.org/10.1073/pnas.1009598107

Koch, R., Ledermann, R., Urwyler, O., Heller, M., Suter, B., 2009. Systematic Functional Analysis of Bicaudal-D Serine Phosphorylation and Intragenic Suppression of a Female Sterile Allele of BicD. PLoS ONE 4, e4552. https://doi.org/10.1371/journal.pone.0004552

Kusevic, D., Kudithipudi, S., Jeltsch, A., 2016. Substrate Specificity of the HEMK2 Protein Glutamine Methyltransferase and Identification of Novel Substrates. J. Biol. Chem. 291, 6124–6133. https://doi.org/10.1074/jbc.M115.711952

Kweon, S.-M., Chen, Y., Moon, E., Kvederaviciutė, K., Klimasauskas, S., Feldman, D.E., 2019. An Adversarial DNA N6-Methyladenine-Sensor Network Preserves Polycomb Silencing. Mol. Cell 74, 1138-1147.e6. https://doi.org/10.1016/j.molcel.2019.03.018

Lacoux, C., Wacheul, L., Saraf, K., Pythoud, N., Huvelle, E., Figaro, S., Graille, M., Carapito, C., Lafontaine, D.L.J., Heurgué-Hamard, V., 2020. The catalytic activity of the translation termination factor methyltransferase

Mtq2-Trm112 complex is required for large ribosomal subunit biogenesis. Nucleic Acids Res. 48, 12310–12325. https://doi.org/10.1093/nar/gkaa972

Lasko, P., 2012. mRNA Localization and Translational Control in Drosophila Oogenesis. Cold Spring Harb. Perspect. Biol. 4, a012294. https://doi.org/10.1101/cshperspect.a012294

Lee, L., Davies, S.E., Liu, J.-L., 2009. The spinal muscular atrophy protein SMN affects Drosophila germline nuclear organization through the U body–P body pathway. Dev. Biol., Special Section: Evolution of Developmental Regulatory Systems 332, 142–155. https://doi.org/10.1016/j.ydbio.2009.05.553

Liao, Y., Smyth, G.K., Shi, W., 2014. featureCounts: an efficient general purpose program for assigning sequence reads to genomic features. Bioinformatics 30, 923–930. https://doi.org/10.1093/bioinformatics/btt656

Lim, L.-X., Isshiki, W., Iki, T., Kawaguchi, S., Kai, T., 2022. The Tudor Domain-Containing Protein, Kotsubu (CG9925), Localizes to the Nuage and Functions in piRNA Biogenesis in D. melanogaster. Front. Mol. Biosci. 9, 818302. https://doi.org/10.3389/fmolb.2022.818302

Liu, P., Nie, S., Li, B., Yang, Z.-Q., Xu, Z.-M., Fei, J., Lin, C., Zeng, R., Xu, G.-L., 2010. Deficiency in a Glutamine-Specific Methyltransferase for Release Factor Causes Mouse Embryonic Lethality. Mol. Cell. Biol. 30, 4245–4253. https://doi.org/10.1128/MCB.00218-10

Love, M.I., Huber, W., Anders, S., 2014. Moderated estimation of fold change and dispersion for RNA-seq data with DESeq2. Genome Biol. 15, 550.

https://doi.org/10.1186/s13059-014-0550-8

McCall, K., 2004. Eggs over easy: cell death in the Drosophila ovary. Dev. Biol. 274, 3–14. https://doi.org/10.1016/j.ydbio.2004.07.017

Metzger, E., Wang, S., Urban, S., Willmann, D., Schmidt, A., Offermann, A., Allen, A., Sum, M., Obier, N., Cottard, F., Ulferts, S., Preca, B.-T., Hermann, B., Maurer, J., Greschik, H., Hornung, V., Einsle, O., Perner, S., Imhof, A., Jung, M., Schüle, R., 2019. KMT9 monomethylates histone H4 lysine 12 and controls proliferation of prostate cancer cells. Nat. Struct. Mol. Biol. 26, 361–371. https://doi.org/10.1038/s41594-019-0219-9

Patil, V.S., Kai, T., 2010. Repression of Retroelements in Drosophila Germline via piRNA Pathway by the Tudor Domain Protein Tejas. Curr. Biol. 20, 724–730. https://doi.org/10.1016/j.cub.2010.02.046

Perkins, L.A., Holderbaum, L., Tao, R., Hu, Y., Sopko, R., McCall, K., Yang-Zhou, D., Flockhart, I., Binari, R., Shim, H.-S., Miller, A., Housden, A., Foos, M., Randkelv, S., Kelley, C., Namgyal, P., Villalta, C., Liu, L.-P., Jiang, X., Huan-Huan, Q., Wang, X., Fujiyama, A., Toyoda, A., Ayers, K., Blum, A., Czech, B., Neumuller, R., Yan, D., Cavallaro, A., Hibbard, K., Hall, D., Cooley, L., Hannon, G.J., Lehmann, R., Parks, A., Mohr, S.E., Ueda, R., Kondo, S., Ni, J.-Q., Perrimon, N., 2015. The Transgenic RNAi Project at Harvard Medical School: Resources and Validation. Genetics 201, 843–852. https://doi.org/10.1534/genetics.115.180208

Pierson, W.E., Hoffer, E.D., Keedy, H.E., Simms, C.L., Dunham, C.M., Zaher, H.S., 2016. Uniformity of Peptide Release Is Maintained by Methylation

of Release Factors. Cell Rep. 17, 11–18. https://doi.org/10.1016/j.celrep.2016.08.085

Ping, X.-L., Sun, B.-F., Wang, L., Xiao, W., Yang, X., Wang, W.-J., Adhikari, S., Shi, Y., Lv, Y., Chen, Y.-S., Zhao, X., Li, A., Yang, Y., Dahal, U., Lou, X.-M., Liu, X., Huang, J., Yuan, W.-P., Zhu, X.-F., Cheng, T., Zhao, Y.-L., Wang, X., Danielsen, J.M.R., Liu, F., Yang, Y.-G., 2014. Mammalian WTAP is a regulatory subunit of the RNA N6-methyladenosine methyltransferase. Cell Res. 24, 177–189. https://doi.org/10.1038/cr.2014.3

Polevoda, B., Span, L., Sherman, F., 2006. The Yeast Translation Release Factors Mrf1p and Sup45p (eRF1) Are Methylated, Respectively, by the Methyltransferases Mtq1p and Mtq2p*. J. Biol. Chem. 281, 2562–2571. https://doi.org/10.1074/jbc.M507651200

Ramazi, S., Zahiri, J., 2021. Post-translational modifications in proteins: resources, tools and prediction methods. Database 2021, baab012. https://doi.org/10.1093/database/baab012

Rastegari, E., Kajal, K., Tan, B.-S., Huang, F., Chen, R.-H., Hsieh, T.-S., Hsu, H.-J., 2020. WD40 protein Wuho controls germline homeostasis via TRIM-NHL tumor suppressor Mei-p26 in *Drosophila*. Development 147, dev182063. https://doi.org/10.1242/dev.182063

Ratel, D., Ravanat, J.-L., Charles, M.-P., Platet, N., Breuillaud, L., Lunardi, J., Berger, F., Wion, D., 2006. Undetectable levels of N6-methyl adenine in mouse DNA: Cloning and analysis of PRED28, a gene coding for a putative mammalian DNA adenine methyltransferase. FEBS Lett. 580, 3179–3184. https://doi.org/10.1016/j.febslet.2006.04.074

Ryšlavá, H., Doubnerová, V., Kavan, D., Vaněk, O., 2013. Effect of posttranslational modifications on enzyme function and assembly. J. Proteomics 92, 80–109. https://doi.org/10.1016/j.jprot.2013.03.025

Schaeffer, V., Althauser, C., Shcherbata, H.R., Deng, W.-M., Ruohola-Baker, H., 2004. Notch-Dependent Fizzy-Related/Hec1/Cdh1 Expression Is Required for the Mitotic-to-Endocycle Transition in Drosophila Follicle Cells. Curr. Biol. 14, 630–636. https://doi.org/10.1016/j.cub.2004.03.040

Schindelin, J., Arganda-Carreras, I., Frise, E., Kaynig, V., Longair, M., Pietzsch, T., Preibisch, S., Rueden, C., Saalfeld, S., Schmid, B., Tinevez, J.-Y., White, D.J., Hartenstein, V., Eliceiri, K., Tomancak, P., Cardona, A., 2012. Fiji - an Open Source platform for biological image analysis. Nat. Methods 9, 10.1038/nmeth.2019. https://doi.org/10.1038/nmeth.2019

Shen, Y., Liu, W., Zuo, J., Han, J., Zhang, Z.C., 2021. Protocol for visualizing newly synthesized proteins in primary mouse hepatocytes. STAR Protoc. 2, 100616. https://doi.org/10.1016/j.xpro.2021.100616

Simms, C.L., Yan, L.L., Zaher, H.S., 2017. Ribosome collision is critical for quality control during no-go decay. Mol. Cell 68, 361-373.e5. https://doi.org/10.1016/j.molcel.2017.08.019

Sprung, R., Chen, Y., Zhang, K., Cheng, D., Zhang, T., Peng, J., Zhao, Y., 2008. Identification and validation of eukaryotic aspartate and glutamate methylation in proteins. J. Proteome Res. 7, 1001–1006. https://doi.org/10.1021/pr0705338

St. Johnston, H.L.-S. and D., 2001. Delta signaling from the germ line controls

the proliferation and differentiation of the somatic follicle cells during Drosophila oogenesis. Genes Dev. 15, 1393–1405. https://doi.org/10.1101/gad.200901

Steinhauer, W.R., Kalfayan, L.J., 1992. A specific ovarian tumor protein isoform is required for efficient differentiation of germ cells in Drosophila oogenesis. Genes Dev. 6, 233–243. https://doi.org/10.1101/gad.6.2.233

Svidritskiy, E., Korostelev, A.A., 2018. Conformational control of translation termination on the 70S ribosome. Struct. Lond. Engl. 1993 26, 821-828.e3. https://doi.org/10.1016/j.str.2018.04.001

Tan, K., Stupack, D.G., Wilkinson, M.F., 2022. Nonsense-mediated RNA decay: an emerging modulator of malignancy. Nat. Rev. Cancer 22, 437–451. https://doi.org/10.1038/s41568-022-00481-2

Thomas, P.D., Ebert, D., Muruganujan, A., Mushayahama, T., Albou, L.-P., Mi, H., 2022. PANTHER: Making genome-scale phylogenetics accessible to all. Protein Sci. 31, 8–22. https://doi.org/10.1002/pro.4218

Tomomatsu S., Watanabe A., Tesina P., Hashimoto S., Ikeuchi K., Li S., Matsuo Y., Beckmann R., Inada T., 2023. Two modes of Cue2-mediated mRNA cleavage with distinct substrate recognition initiate no-go decay. Nucleic Acids Res. 51, 253–270. https://doi.org/10.1093/nar/gkac1172

Tsuboi, T., Kuroha, K., Kudo, K., Makino, S., Inoue, E., Kashima, I., Inada, T., 2012. Dom34:Hbs1 Plays a General Role in Quality-Control Systems by Dissociation of a Stalled Ribosome at the 3′ End of Aberrant mRNA. Mol. Cell 46, 518–529. https://doi.org/10.1016/j.molcel.2012.03.013

Van Buskirk, C., Schüpbach, T., 2002. half pint Regulates Alternative Splice

Site Selection in Drosophila. Dev. Cell 2, 343–353. https://doi.org/10.1016/S1534-5807(02)00128-4

Wall, A.A., Phillips, A.M., Kelly, L.E., 2005. Effective Translation of the Second Cistron in Two Drosophila Dicistronic Transcripts Is Determined by the Absence of In-frame AUG Codons in the First Cistron*. J. Biol. Chem. 280, 27670–27678. https://doi.org/10.1074/jbc.M500255200

Wang, X., Feng, J., Xue, Y., Guan, Z., Zhang, D., Liu, Z., Gong, Z., Wang, Q., Huang, J., Tang, C., Zou, T., Yin, P., 2016. Structural basis of N6-adenosine methylation by the METTL3–METTL14 complex. Nature 534, 575–578. https://doi.org/10.1038/nature18298

Werz, C., Lee, T.V., Lee, P.L., Lackey, M., Bolduc, C., Stein, D.S., Bergmann, A., 2005. Mis-specified cells die by an active gene-directed process, and inhibition of this death results in cell fate transformation in *Drosophila*. Development 132, 5343–5352. https://doi.org/10.1242/dev.02150

Woodcock, C.B., Yu, D., Zhang, X., Cheng, X., 2019. Human HemK2/KMT9/N6AMT1 is an active protein methyltransferase, but does not act on DNA in vitro, in the presence of Trm112. Cell Discov. 5, 50. https://doi.org/10.1038/s41421-019-0119-5

Wu, C.C.-C., Peterson, A., Zinshteyn, B., Regot, S., Green, R., 2020. Ribosome Collisions Trigger General Stress Responses to Regulate Cell Fate. Cell 182, 404-416.e14. https://doi.org/10.1016/j.cell.2020.06.006

Xiao, C.-L., Zhu, S., He, M., Chen, D., Zhang, Q., Chen, Y., Yu, G., Liu, J., Xie, S.-Q., Luo, F., Liang, Z., Wang, D.-P., Bo, X.-C., Gu, X.-F., Wang, K.,

Yan, G.-R., 2018. N6-Methyladenine DNA Modification in the Human Genome. Mol. Cell 71, 306-318.e7. https://doi.org/10.1016/j.molcel.2018.06.015

Zhao, Y., Garcia, B.A., 2015. Comprehensive Catalog of Currently Documented Histone Modifications. Cold Spring Harb. Perspect. Biol. 7, a025064. https://doi.org/10.1101/cshperspect.a025064

Legends

Figure 1. HemK2 is essential for female germline development and functions in mid-oogenesis.

(A) Schematic representation of *Drosophila* oogenesis. The ovariole consists of the germarium, situated at the anterior tip of the ovariole, followed by a series of sequential stages of egg chamber development. The 16-cell germline cyst originates from the germarium and is encapsulated by a monolayer of somatic follicle cells to generate an egg chamber. One of the 16-cells is identified as the oocyte, which will eventually develop into a mature egg. The developmental checkpoint before the vitellogenesis phases, known as mid-oogenesis, is characterized at stage 7/8. **(B)** Morphological images of control and HemK2 germline knockdown (GLKD) ovaries. *hemk2*-GLKD causes female sterility marked by developmental arrest of egg chambers at stages 7-8 and disruption of vitellogenesis. scale bar is 250 µm. **(C)** qRT-PCR validation of knockdown efficiency in *hemk2*-GLKD ovaries. All values are normalized to *rp49* with *tubulin* as a control. Error bars indicate standard deviation (n=3). **(D)** Egg laying and hatching analysis. Sterility in *hemk2*-GLKD was rescued by wild-type FLAG-tagged HemK2 transgene expression driven by germline driver *NGT40* and *nosGal4-VP16*. Eggs are produced by 3 females every day (n=3). Error bars indicate standard deviation. **(E)** Staining of FLAG-tagged HemK2 (Green) and DAPI (Blue) for DNA in ovaries with each indicated genotype as in (D). Arrows indicate the degenerated egg chambers

in HemK2-GLKD and later stage egg chambers in FLAG-HemK2 transgene expression. All scale bars are 50 µm. **(F)** Western blots detecting FLAG showing the germline expression of FLAG-HemK2 wildtype in ovary lysate. Tubulin was used as the loading control.

Figure 2. HemK2 functions for multiple morphological aspects of *Drosophila* germline.

(A) Immunostaining of pH3 (Red) for mitosis and DAPI (Blue) for DNA in ovaries (left panel). The hyperplasia of the posterior follicle cells in *hemk2*-GLKD is denoted with dotted rectangle (upper right panel). All scale bars are 20 µm. % of ovarioles with single or multi-layered follicle cells is quantified (right panel, n=100). **(B)** Immunostaining of Fibrillarin (Green) for nucleolus and DAPI (Blue) for DNA in stage7/8 egg chambers. Inset shows a magnified image of nurse cell nucleus with dispersed or undispersed chromosomes. All scale bars are 10 µm. **(C)** qRT-PCR analysis shows expression level of each chromosome dispersion associated genes. Error bars indicate standard deviation (n=3). **(D)** Immunostaining of *p53* (Green) for apoptosis and DAPI (Blue) for DNA in ovaries (left panel). Arrows indicate the accumulation of *p53* signals in the nuclei of nurse cells. All scale bars are 20 µm. % of ovarioles with or without *p53* signals is quantified (right panel, n=100).

Figure 3. The methylation of eRF1 was reduced by *hemk2*-GLKD significantly.

(A) Immunoprecipitation of endogenous eRF1 in ovaries. Western blots detecting N5-methyl-glutamine (Methyl-Q: bottom panel) showed the reduction of eRF1 methylation by *hemk2*-GLKD. Heterozygous ovaries were used as the control. Methyl-Q band intensity normalized to eRF1 was quantified (right panel). Error bars indicate standard deviation (n=3), *p*-value is shown (unpaired *t*-test). **(B)** Immunostaining of methyl-eRF1 (Green) and eRF1 (Red) in *hemk2*-GLKD ovaries. Allows show the cytosol of the germline cells. All scale bars are 20 µm. **(C)** Immunoprecipitation of FLAG-eRF1 expressed in germline cells in ovaries. *Matα-tub-Gal4* was used to drive the germline expression of FLAG-eRF1. Western blots detecting Methyl-Q showed the significant reduction of FLAG-eRF1 methylation by *hemk2*-GLKD. Asterisks indicate the nonspecific band. Quantification of Methyl-Q band intensity normalized to FLAG-eRF1 (right panel) was performed as in (A). Error bars indicate standard deviation (n=3), *p*-value is shown (unpaired *t*-test). **(D)** Immunoprecipitation of FLAG-eRF1 Q185A in S2 cells. Western blots detecting Methyl-Q showing a scanty of methylation in both conditions. Asterisks indicate the nonspecific band.

Figure 4. eRF1 methylation is required for *hemk2* function.

(A) A schematic diagram showing MTase domain of *Drosophila* HemK2. Alignment shows that the NPPY motif in the substrate binding pocket is highly conserved among different species and HemK2 mutants were generated with Asn116 to Ala (N116A) and Tyr119 to Ala (Y119A), respectively. **(B)** The crystal structure of the human HemK2-TRMT112 bound with methyl-glutamine (Methyl-Q) and S-adenosylhomocysteine (SAH) (Gao et al., 2020). Only active site around Methyl-Q is shown. HemK2 and Methyl-Q are shown in gray and green, respectively. N122 and Y125 are correspond to N116 and Y119 in *Drosophila* HemK2, respectively. Hydrogen bonds around Methyl-Q product are also shown. **(C)** Immunostaining of FLAG-tagged HemK2 variants (Green) and DAPI (Blue) for DNA in ovaries with each indicated genotype. The defects in *hemk2*-GLKD were rescued by transgene expression of the N116A, but not Y119A HemK2 mutant. All scale bars are 50 µm. **(D)** Egg laying and hatching analysis of each indicated genotype as in (C). Eggs are produced by 3 females every day (n=3). Error bars indicate standard deviation. **(E)** Immunoprecipitation of FLAG-eRF1 in S2 cells. Myc-HemK2 mutants and FLAG-eRF1 were co-transfected with or without HemK2 knockdown (KD). Western blots detecting Methyl-Q showing the reduction of FLAG-eRF1 methylation in *hemk2*-KD was rescued by expression of HemK2 wildtype and N116A, but not Y119A HemK2 mutant. Quantification of Methyl-Q band intensity normalized to FLAG-eRF1 was performed (bottom panel).

Figure 5. eRF1 methylation ensures proper progression of oogenesis and was needed for efficient translation.

(A) Morphological images of control and *eRF1*-GLKD ovaries. Scale bar is 250 µm. **(B)** Egg laying and hatching analysis of each indicated genotype. Eggs are produced by 3 females every day (n=3). Error bars indicate standard deviation. **(C)** Immunostaining of FLAG-tagged eRF1 WT/Q185A (Green), Vas (Red) for germline cells and DAPI (Blue) for DNA in ovaries with each indicated genotype as in (B). The defects in *eRF1*-GLKD were rescued by transgene expression of wildtype eRF1 but not Q185A eRF1 mutant. All scale bars are 20 µm. **(D)** Immunostaining of FLAG-tagged eRF1 Q185A (Red) and DAPI (Blue) for DNA in ovaries. The overexpression of FLAG-eRF1 Q185A in wildtype phenocopied *hemk2*-GLKD. Arrows indicate the dying egg chambers. All scale bars are 50 µm. **(E)** Homopropargylglycine (HPG) protein synthesis assay in ovaried with each indicated genotype (Green in left panels). FLAG (Red) showing transgene expression was immunostained in parallel. All scale bars are 20 µm. Quantification of HPG signal intensity in each genotype of the left panels is shown in the right panel. Representative images were measured (n=5). Error bars indicate standard deviation.

Figure 6. HemK2 knockdown resulted the mRNA reduction in germline

cells and ribosome stalling.

(A) GO analysis of the downregulated genes in *hemk2*-GLKD ovary. Overrepresentation of the GO biological process term was tested by PANTHER (version 18.0). The fold enrichments were plotted and colored according to their FDR values. **(B)** GO terms of the upregulated genes in *hemk2*-GLKD ovary analyzed as in (A). **(C)** Volcano plot of the germline-enriched genes in *hemk2*-GLKD ovaries. (orange: p-value < 0.05 and log2FC **<** -1 or **>** 1). Cell type-enriched genes are defined according to the single cell mRNA-seq analysis of *Drosophila* ovaries (Jevitt et al., 2020). **(D)** Log2-fold changes of cell-type enriched coding genes in *hemk2*-GLKD ovaries compared with the control (average +/- standard deviation). **(E)** Profiles of ribosomes in ovarian lysates of the control (blue), *hemk2*-GLKD (red), and double germline knockdown of *hemk2* and *ski8* (green). The mRNA-bound monosomes and disomes were separated by the sucrose gradient sedimentation. The elution profiles were recorded by the absorbance at 254 nm and normalized by the monosome peaks in each sample. The disome peaks are shown in the inset.

Figure 7. Defects during oogenesis in *hemk2*-GLKD were rescued by blocking of the no-go decay (NGD) pathway.

(A) Immunostaining of DAPI (Blue) for DNA in ovaries with each indicated genotype. The defects in *hemk2*-GLKD were rescued by double knockdown of

ski8 or *pelo*, but not *CG7139* or *upf3*. All scale bars are 50µm. **(B)** Egg laying and hatching analysis of each indicated genotype as in (A). Eggs are produced by 3 females every day (n=3). Error bars indicate standard deviation. **(C)** HPG protein synthesis assay in ovaried with each indicated genotype as in (A). All scale bars are 20 µm. **(D)** % of ovarioles labeled with HPG positive is quantified (left panel, n=100). Quantification of HPG signal intensity in each genotype in (C) is shown in the right panel. Representative images were measured (n=5). Error bars indicate standard deviation.

Supplementary Legends

Figure S1. HemK2 plays a predominant role not only in germline but also in somatic cells.

(A) A schematic drawing of *Drosophila* HemK2/Snapin locus. The primers of Snapin dsRNA and HemK2 qPCR are illustrated (bottom). **(B)** Egg laying and hatching analysis. Sterility in HemK2 somatic knockdown (STKD) was rescued by wild-type FLAG-tagged HemK2 transgene expression driven by somatic driver *traffic jam-Gal4*. Eggs are produced by 3 females every day (n=3). Error bars indicate standard deviation**. (C)** Immunostaining of FLAG-tagged HemK2 (Green) and DAPI (Blue) for DNA in ovaries with each indicated genotype as in (B). Arrows indicate the degenerated egg chambers in HemK2-STKD and later stage egg chambers in FLAG-HemK2 transgene expression. All scale bars are 50 µm. **(D)** Egg laying and hatching analysis. Sterility in *hemk2/snapin*-GLKD was not rescued by Snapin transgene expression driven by germline driver *NGT40 and nosGal4-VP16*. Eggs are produced by 3 females every day (n=3). Error bars indicate standard deviation. **(E)** Immunostaining of FLAG-tagged Snapin (Green) and DAPI (Blue) for DNA in ovaries with each indicated genotype as in (D). All scale bars are 50 µm. **(F)** qRT-PCR validation of knockdown efficiency in *hemk2*-GLKD testes. All values are normalized to *rp49* with *tubulin* as a control. Error bars indicate standard deviation (n=3). **(G)** Egg laying and hatching analysis in testes. Eggs are produced by 3 *yw* females every day mated with the indicated males (n=3). Error bars indicate

standard deviation.

Figure S2. The defects in *hemk2*-GLKD were rescued by the repression of cell death partially.

(A) Immunostaining of FLAG-tagged otu104 (Red), Fibrillarin (Green) for nucleolus and DAPI (Blue) for DNA in ovaries with each indicated genotype (left panel). The chromosomal dispersion defect in *hemk2*-GLKD was partially rescued by transgene expression of *otu*104 driven by germline driver *NGT40 and nosGal4-VP16*. All scale bars are 20 µm. % of ovarioles with dispersed or undispersed chromosomes is quantified (right panel, n=100, stage 6 and older egg chambers). **(B)** Immunostaining of Fibrillarin (Green) for nucleolus and DAPI (Blue) for DNA in egg chambers with each indicated genotype. The stages of egg chambers are determined and labeled (bottom). **(C)** Egg laying and hatching analysis of each indicated genotype as in (B). Eggs are produced by 3 females every day (n=3). Error bars indicate standard deviation.

Figure S3. DNA 6mA and histone H4K12 remained unaffected by *hemk2*-GLKD.

(A) Immunostaining of Vas (Red) for germline cells, DNA N6-adenine (6mA) (Green) and DAPI (Blue) for DNA in ovaries. DNA 6mA was unaffected by *hemk2*-GLKD. All scale bars are 20 µm. **(B)** Immunoblotting of histone H4 and

H4K12met in ovary lysate. Tubulin was used as the loading control.

Figure S4. eRF1 methylation is uniquely catalyzed by HemK2.

(A) Western blots detecting FLAG showing the germline expression of FLAG-HemK2 N116A and Y119A mutants in ovary lysate. Tubulin was used as the loading control. **(B)** Immunoprecipitation of FLAG-eRF1 in S2 cells. Myc-HemK1/HemK2 and FLAG-eRF1 were co-transfected with or without *hemk2* KD. Western blots detecting Methyl-Q showing the reduction of FLAG-eRF1 methylation in *hemk2*-KD was rescued by expression of HemK2 but not HemK1. Quantification of Methyl-Q band intensity normalized to FLAG-eRF1was performed (bottom panel).

Figure S5. The overexpression of FLAG-eRF1 Q185A in wildtype phenocopied *hemk2*-GLKD.

(A) Western blots detecting eRF1 showing the expression of endogenous eRF1 and FLAG-eRF1 Q185A in ovary lysate. *Matα-tub-Gal4* was used to drive the germline expression of FLAG-eRF1 Q185A. Tubulin was used as the loading control. **(B)** Egg laying and hatching analysis of each indicated genotype. Eggs are produced by 3 females every day (n=3). Error bars indicate standard deviation. **(C)** Immunostaining of p53 (Green) for apoptosis and DAPI (Blue) for DNA in ovaries (left panel). The overexpression of

FLAG-eRF1 Q185A in wildtype phenocopied *hemk2*-GLKD in cell death. Arrows indicate the accumulation of *p53* signals in the nuclei of nurse cells. All scale bars are 20 µm. % of ovarioles with or without p53 signals is quantified (right panel, n=100). **(D)** HPG protein synthesis assay in ovaried (left panels). FLAG (Red) showing transgene expression was immunostained in parallel. All scale bars are 20 µm. Quantification of HPG signal intensity in each genotype of the left panels is shown in the right panel. Representative images were measured (n=5), *p*-values are shown (unpaired *t*-test). Error bars indicate standard deviation.

Figure S6. *hemk2* knockdown resulted the mRNA reduction in germline cells, but not in somatic cells.

(A-E) Volcano plot of the cell type-enriched genes in *hemk2*-GLKD ovaries. (orange: p-value < 0.05 and log2FC **<** -1 or **>** 1). Cell type-enriched genes are defined according to the single cell mRNA-seq analysis of *Drosophila* ovaries (Jevitt et al., 2020). Somatic germarium (A), Polar cells (B), Stalk cells (C), pre-follicle cells (D), and mitotic follicle cells (E). **(F, G)** Log2-fold changes of cell-type enriched coding genes in *hemk2-ski8*-DGKD (F) and in *hemk2-pelo*-DGKD (G) ovaries compared with the control (average +/- standard deviation).

Figure S7. Validations of the knockdown efficiency for each mRNA decay factor. (A) qRT-PCR was performed to validate the knockdown of *hemk2*, *ski8*, *pelo*, *cg7139*, and *upf3*. Error bars indicate standard deviation. (B) *CG7139* is a *Drosophila* homolog of *nonu-1*/*cue2*. Smr nuclease and AAA_33 kinase domains showed the 30% and 20% identity, respectively.

Figure 1

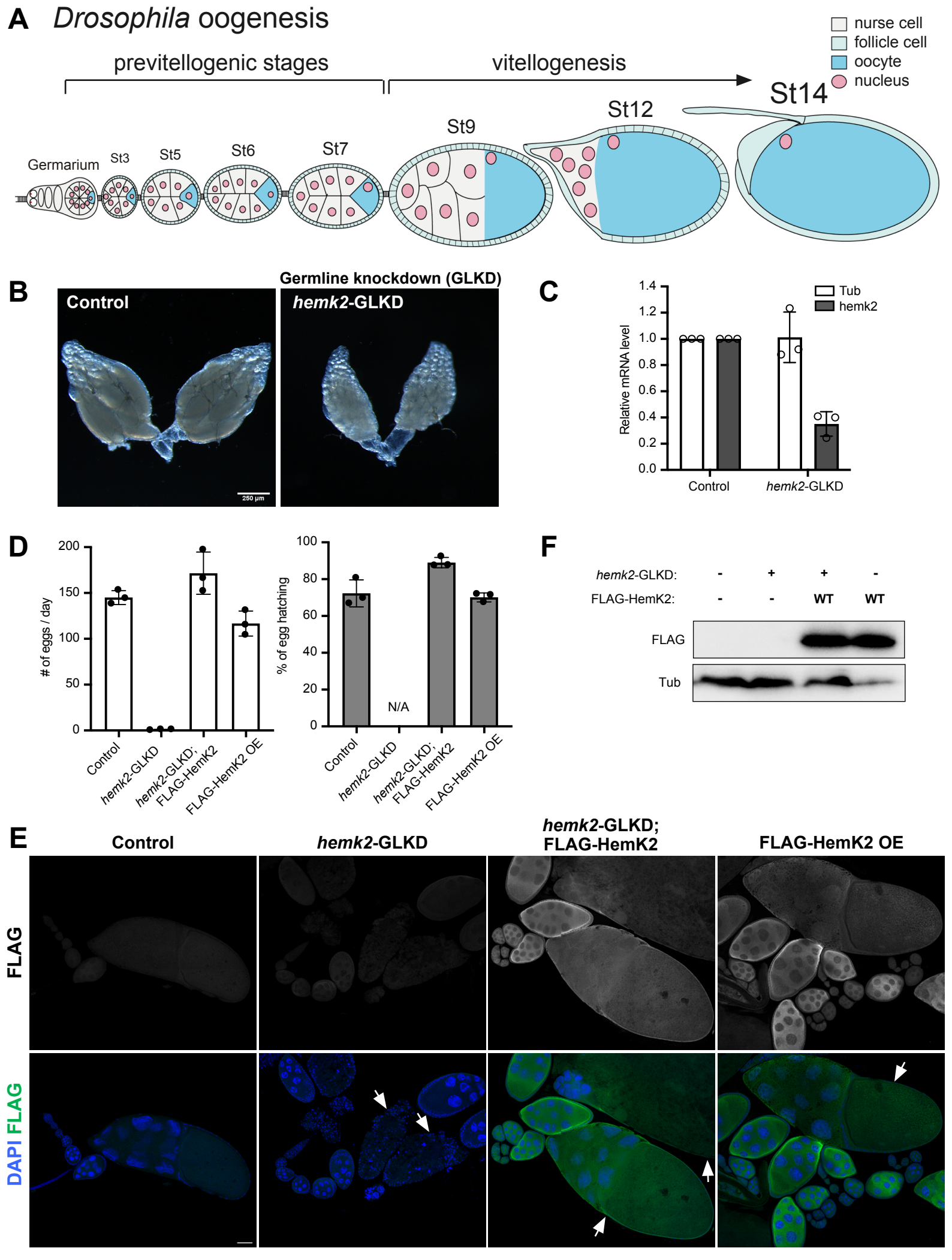
A
Drosophila oogenesis
previtellogenic stages
vitellogenesis
nurse cell
follicle cell
oocyte
nucleus
Germarium
St3
St5
St6
St7
St9
St12
St14
B
Germline knockdown (GLKD)
Control
hemk2-GLKD
250 µm
C
Tub
hemk2
Relative mRNA level
1.4
1.2
1.0
0.8
0.6
0.4
0.2
0.0
Control
hemk2-GLKD
D
# of eggs / day
200
150
100
50
0
Control
hemk2-GLKD
hemk2-GLKD; FLAG-HemK2
FLAG-HemK2 OE
% of egg hatching
100
80
60
40
20
0
N/A
Control
hemk2-GLKD
hemk2-GLKD; FLAG-HemK2
FLAG-HemK2 OE
F
hemk2-GLKD: - + + -
FLAG-HemK2: - - WT WT
FLAG
Tub
E
Control
hemk2-GLKD
hemk2-GLKD; FLAG-HemK2
FLAG-HemK2 OE
FLAG
DAPI FLAG

Figure 2

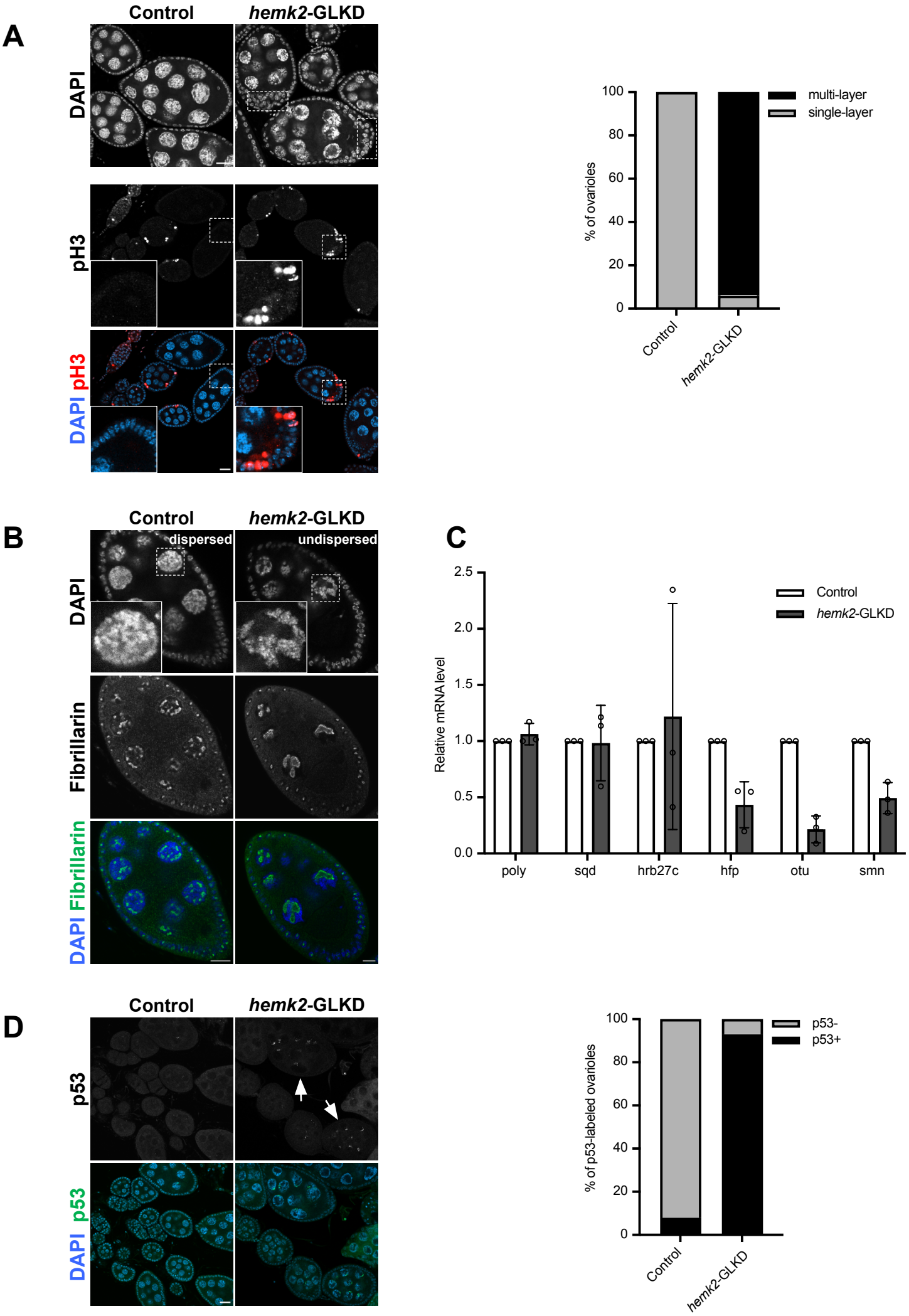
A
Control
hemk2-GLKD
DAPI
pH3
DAPI pH3
multi-layer
single-layer
% of ovarioles
100
80
60
40
20
0
Control
hemk2-GLKD
B
Control
hemk2-GLKD
dispersed
undispersed
DAPI
Fibrillarin
DAPI Fibrillarin
C
Control
hemk2-GLKD
Relative mRNA level
2.5
2.0
1.5
1.0
0.5
0.0
poly
sqd
hrb27c
hfp
otu
smn
D
Control
hemk2-GLKD
p53
DAPI p53
p53-
p53+
% of p53-labeled ovarioles
100
80
60
40
20
0
Control
hemk2-GLKD

Figure 3

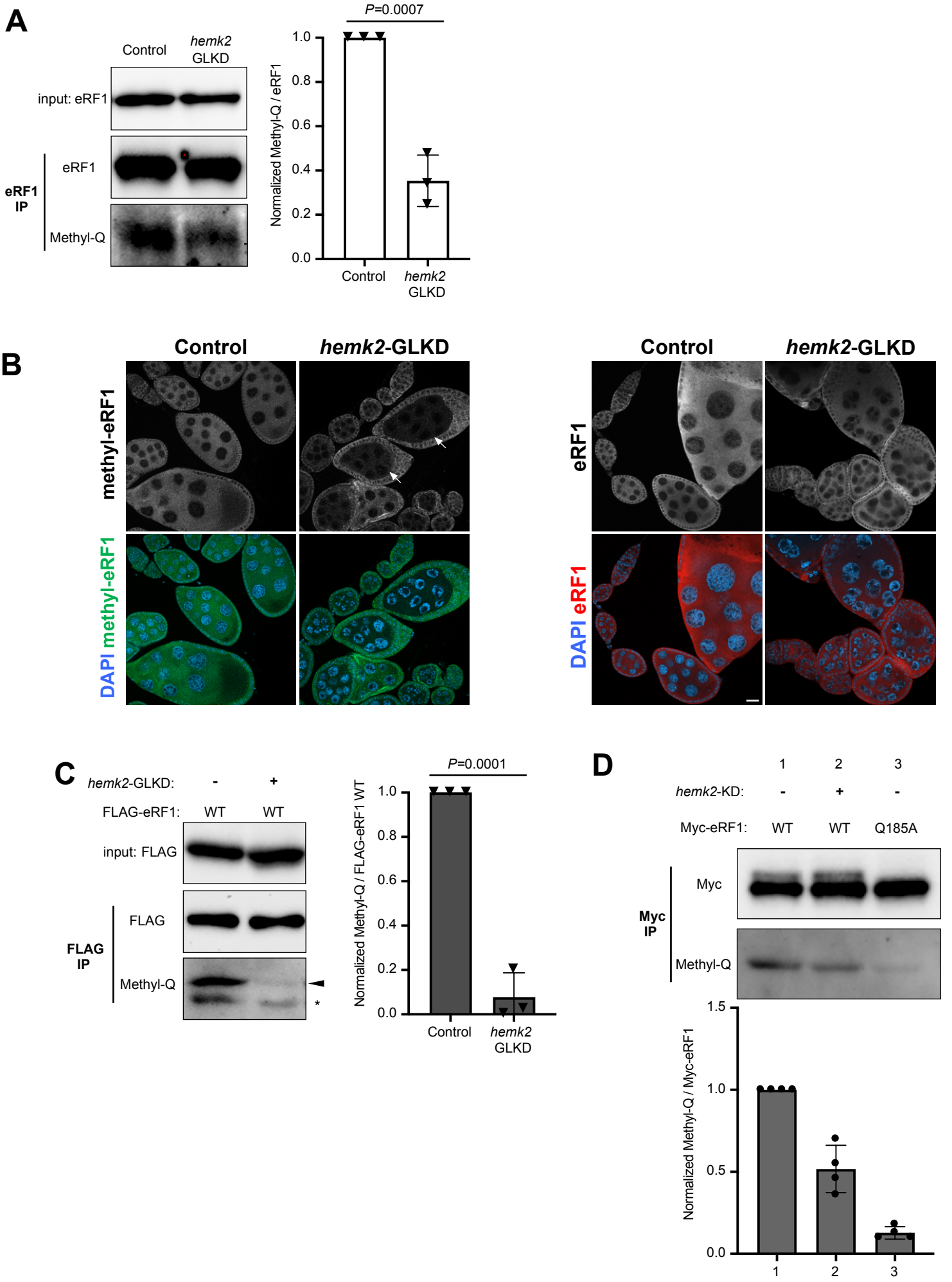
A
Control
hemk2 GLKD
input: eRF1
eRF1
eRF1 IP
Methyl-Q
P=0.0007
Normalized Methyl-Q / eRF1
1.0
0.8
0.6
0.4
0.2
0.0
Control
hemk2 GLKD
B
Control
hemk2-GLKD
methyl-eRF1
DAPI methyl-eRF1
Control
hemk2-GLKD
eRF1
DAPI eRF1
C
hemk2-GLKD: - +
FLAG-eRF1: WT WT
input: FLAG
FLAG
FLAG IP
Methyl-Q
*
P=0.0001
Normalized Methyl-Q / FLAG-eRF1 WT
1.0
0.8
0.6
0.4
0.2
0.0
Control
hemk2 GLKD
D
1 2 3
hemk2-KD: - + -
Myc-eRF1: WT WT Q185A
Myc
Myc IP
Methyl-Q
Normalized Methyl-Q / Myc-eRF1
1.5
1.0
0.5
0.0
1
2
3

Figure 4

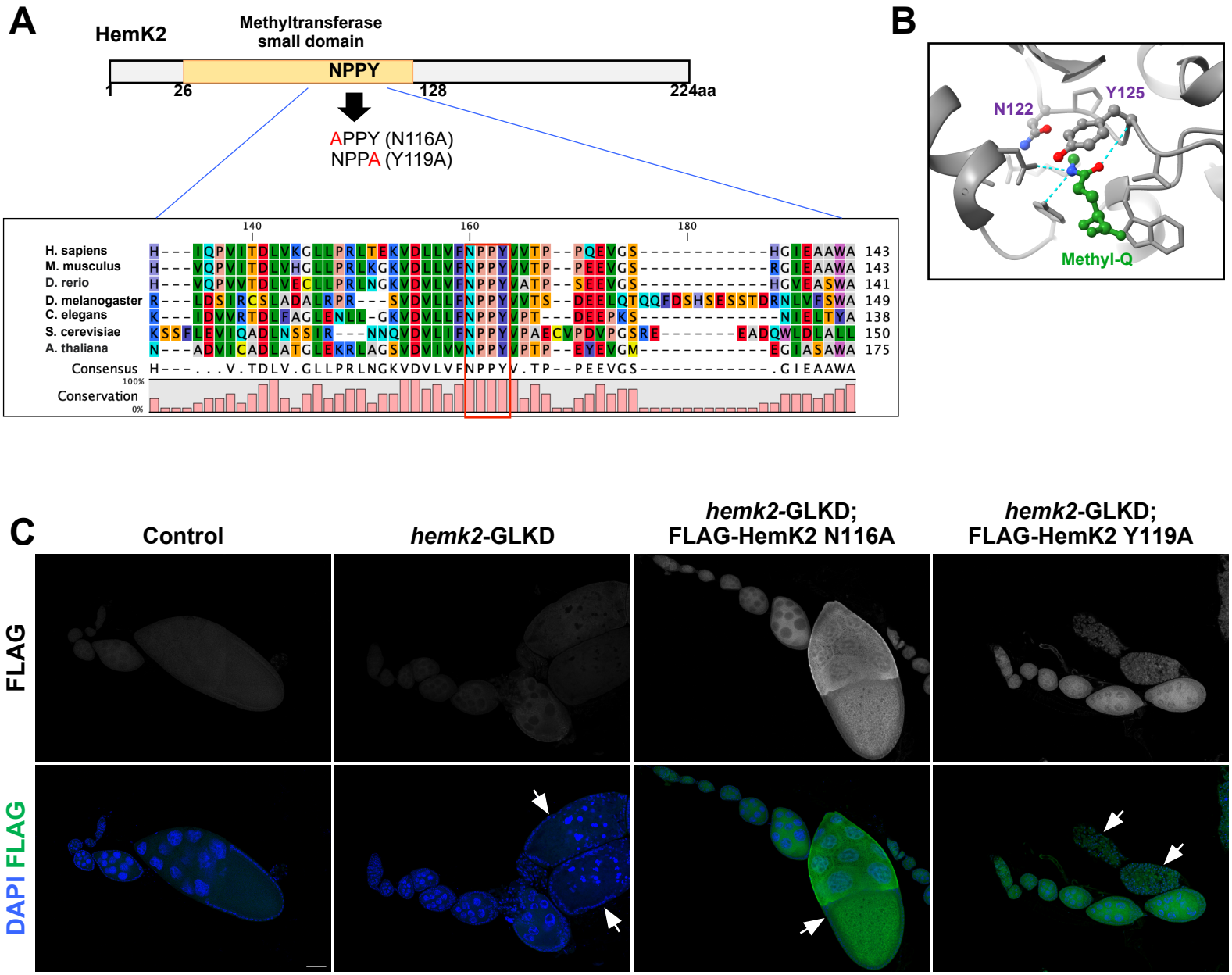
A
HemK2
Methyltransferase small domain
NPPY
1
26
128
224aa
APPY (N116A)
NPPA (Y119A)
H. sapiens
M. musculus
D. rerio
D. melanogaster
C. elegans
S. cerevisiae
A. thaliana
Consensus
Conservation
B
N122
Y125
Methyl-Q
C
Control
hemk2-GLKD
hemk2-GLKD; FLAG-HemK2 N116A
hemk2-GLKD; FLAG-HemK2 Y119A
FLAG
DAPI FLAG
D
# of eggs / day
% of egg hatching
N/A
N/A
Control
hemk2-GLKD
hemk2-GLKD; FLAG-HemK2 N116A
hemk2-GLKD; FLAG-HemK2 Y119A
E
hemk2-KD:
FLAG-HemK2:
Myc-eRF1:
WT
N116A
Y119A
Input:
Myc
FLAG
Myc IP
Methyl-Q
Normalized Methyl-Q / Myc-eRF1

Figure 5

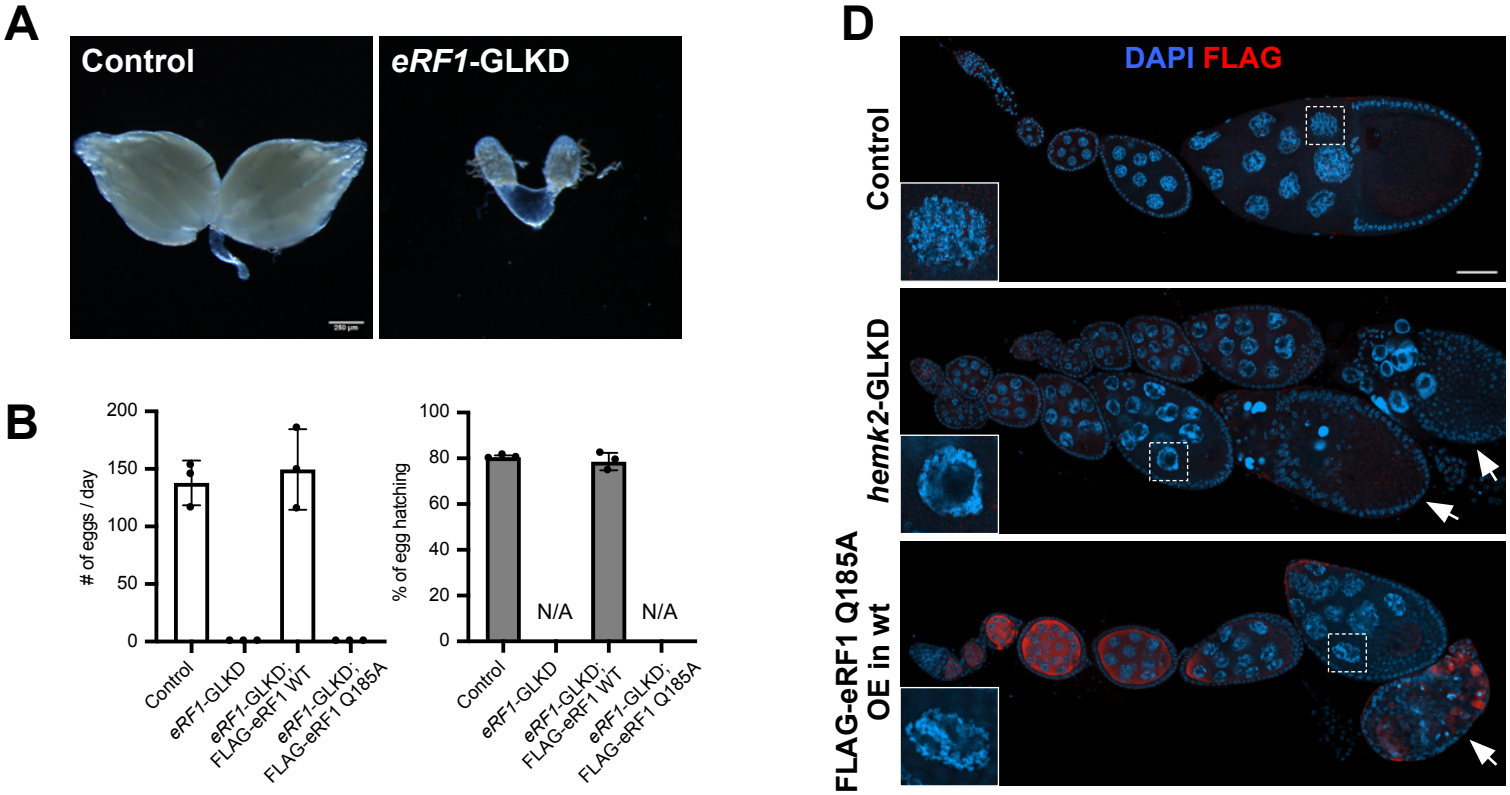
A
Control
eRF1-GLKD
B
# of eggs / day
200
150
100
50
0
Control
eRF1-GLKD
eRF1-GLKD; FLAG-eRF1 WT
eRF1-GLKD; FLAG-eRF1 Q185A
% of egg hatching
100
80
60
40
20
0
N/A
N/A
D
DAPI FLAG
Control
hemk2-GLKD
FLAG-eRF1 Q185A OE in wt

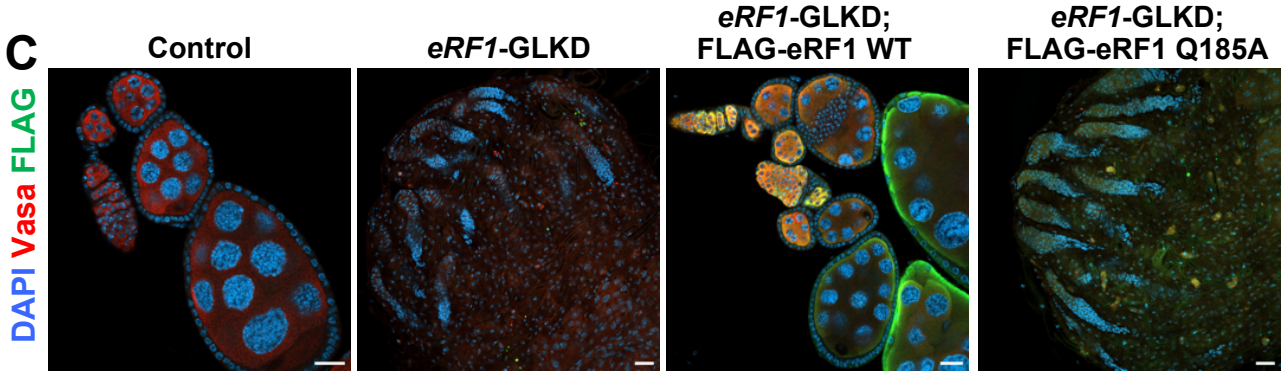
C
Control
eRF1-GLKD
eRF1-GLKD; FLAG-eRF1 WT
eRF1-GLKD; FLAG-eRF1 Q185A
DAPI Vasa FLAG

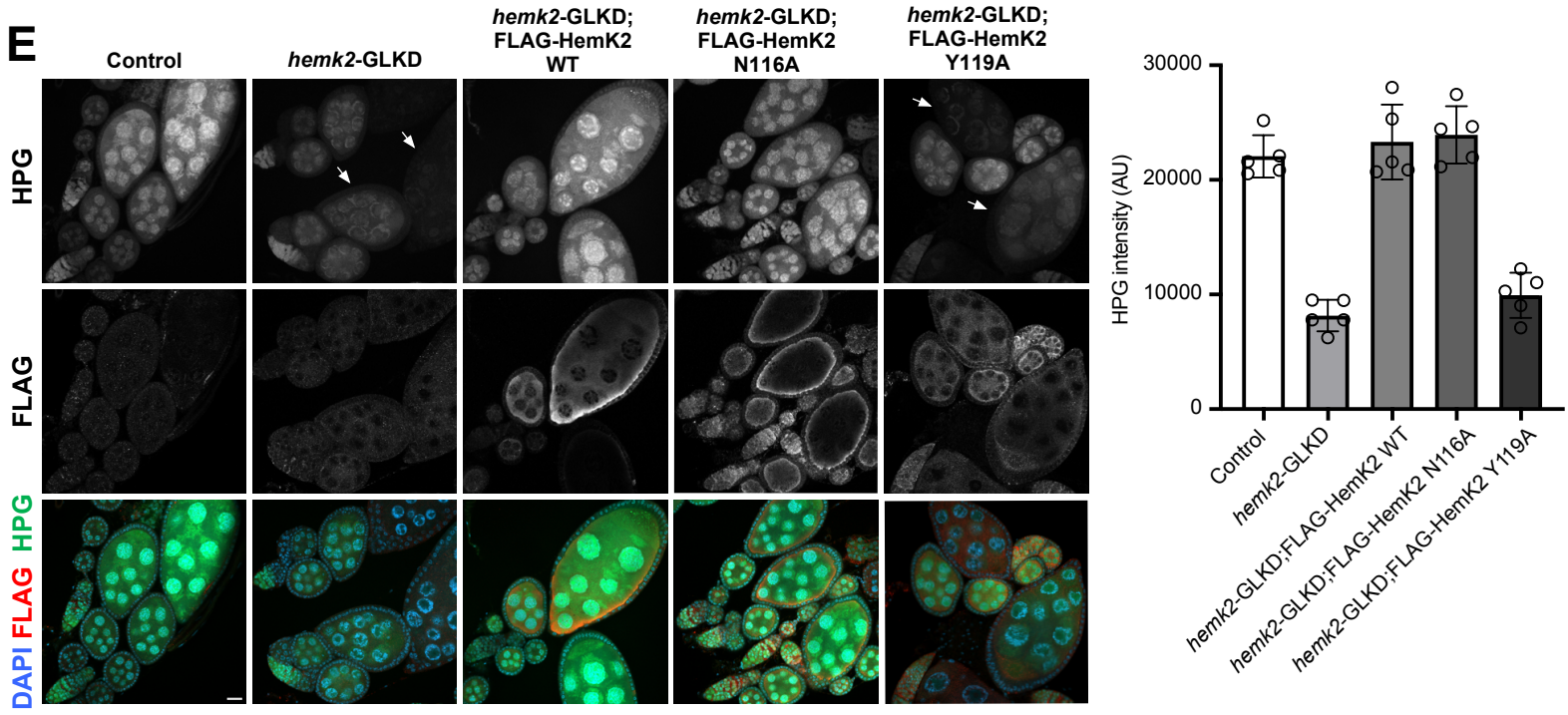
E
Control
hemk2-GLKD
hemk2-GLKD; FLAG-HemK2 WT
hemk2-GLKD; FLAG-HemK2 N116A
hemk2-GLKD; FLAG-HemK2 Y119A
HPG
FLAG
DAPI FLAG HPG
HPG intensity (AU)
30000
20000
10000
0
Control
hemk2-GLKD
hemk2-GLKD;FLAG-HemK2 WT
hemk2-GLKD;FLAG-HemK2 N116A
hemk2-GLKD;FLAG-HemK2 Y119A

Figure 6

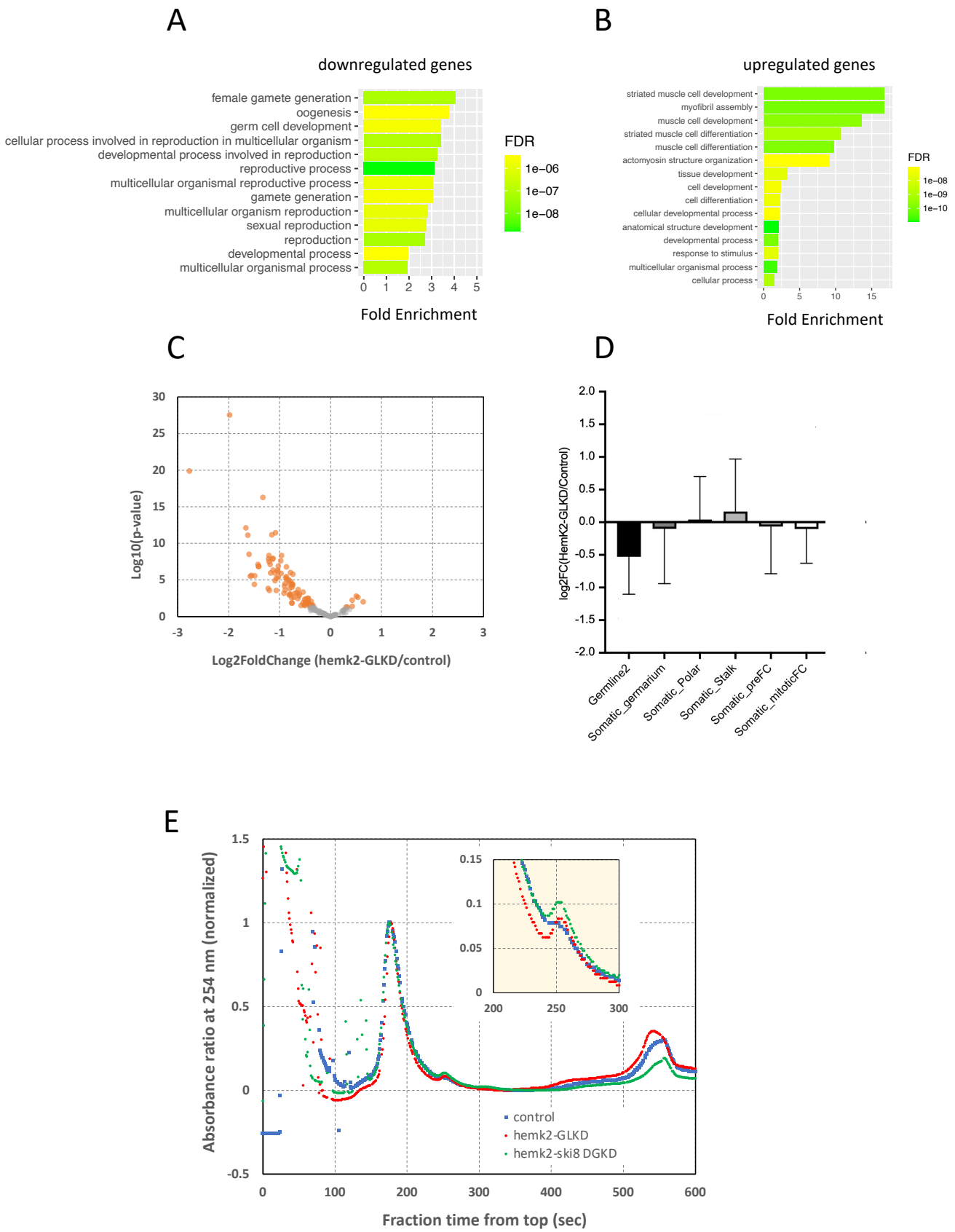
A
downregulated genes
female gamete generation
oogenesis
germ cell development
cellular process involved in reproduction in multicellular organism
developmental process involved in reproduction
reproductive process
multicellular organismal reproductive process
gamete generation
multicellular organism reproduction
sexual reproduction
reproduction
developmental process
multicellular organismal process
0 1 2 3 4 5
Fold Enrichment
FDR
1e−06
1e−07
1e−08
B
upregulated genes
striated muscle cell development
myofibril assembly
muscle cell development
striated muscle cell differentiation
muscle cell differentiation
actomyosin structure organization
tissue development
cell development
cell differentiation
cellular developmental process
anatomical structure development
developmental process
response to stimulus
multicellular organismal process
cellular process
0 5 10 15
Fold Enrichment
FDR
1e−08
1e−09
1e−10
C
Log10(p-value)
30 25 20 15 10 5 0
-3 -2 -1 0 1 2 3
Log2FoldChange (hemk2-GLKD/control)
D
log2FC(HemK2-GLKD/Control)
2.0 1.5 1.0 0.5 0.0 -0.5 -1.0 -1.5 -2.0
Germline2
Somatic_germarium
Somatic_Polar
Somatic_Stalk
Somatic_preFC
Somatic_mitoticFC
E
Absorbance ratio at 254 nm (normalized)
1.5 1 0.5 0 -0.5
0 100 200 300 400 500 600
Fraction time from top (sec)
0.15 0.1 0.05 0
200 250 300
control
hemk2-GLKD
hemk2-ski8 DGKD

Figure 7

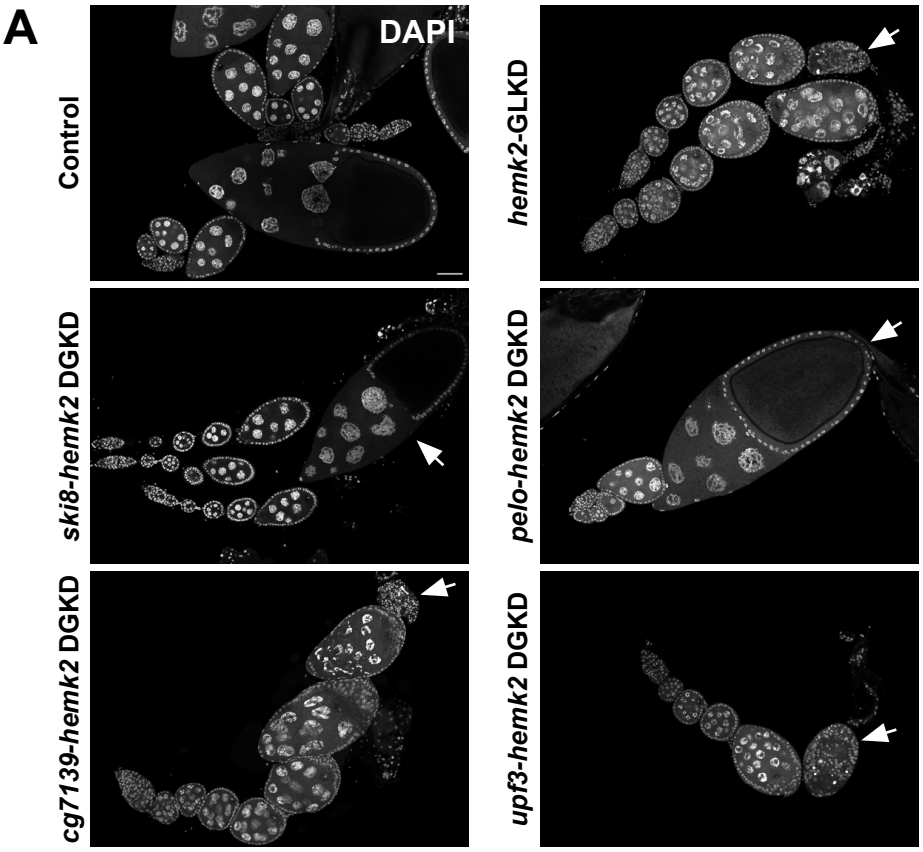
A
DAPI
Control
hemk2-GLKD
ski8-hemk2 DGKD
pelo-hemk2 DGKD
cg7139-hemk2 DGKD
upf3-hemk2 DGKD

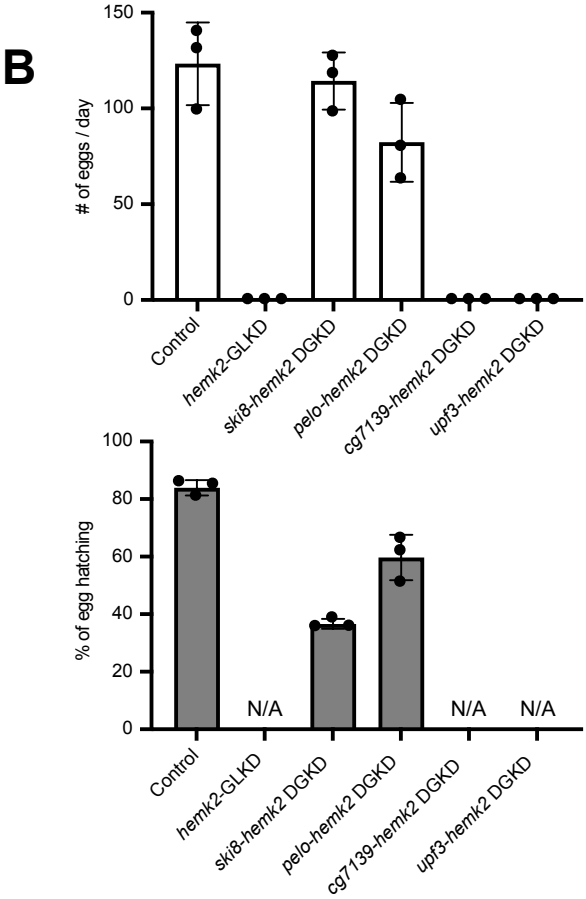
B
# of eggs / day
150
100
50
0
Control
hemk2-GLKD
ski8-hemk2 DGKD
pelo-hemk2 DGKD
cg7139-hemk2 DGKD
upf3-hemk2 DGKD
% of egg hatching
100
80
60
40
20
0
N/A
N/A
N/A

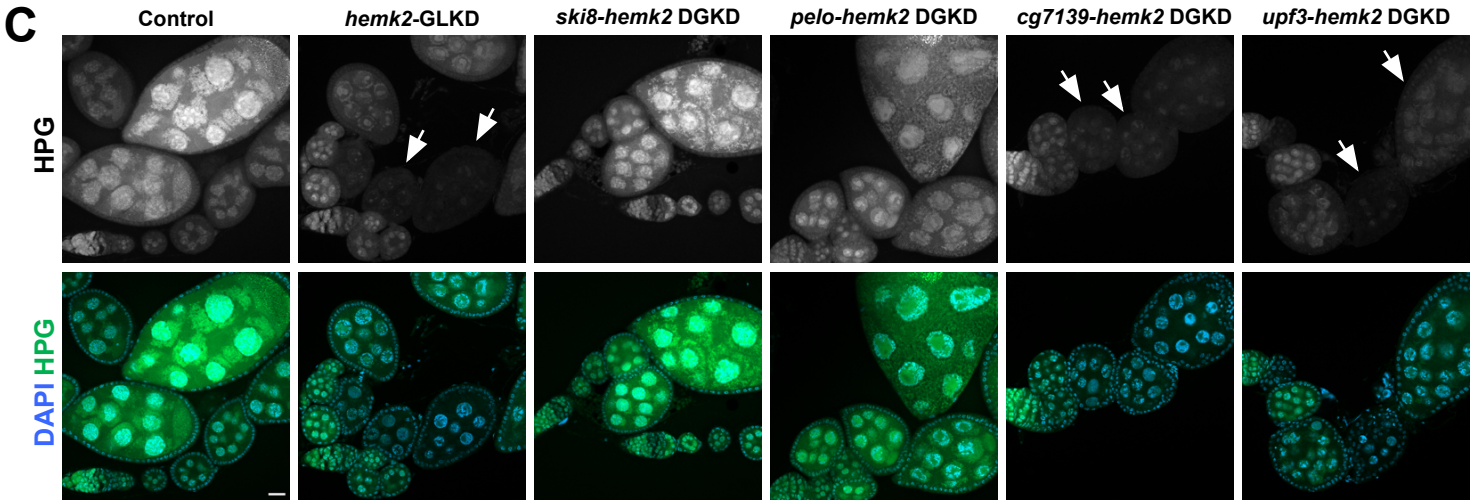
C
Control
hemk2-GLKD
ski8-hemk2 DGKD
pelo-hemk2 DGKD
cg7139-hemk2 DGKD
upf3-hemk2 DGKD
HPG
DAPI HPG

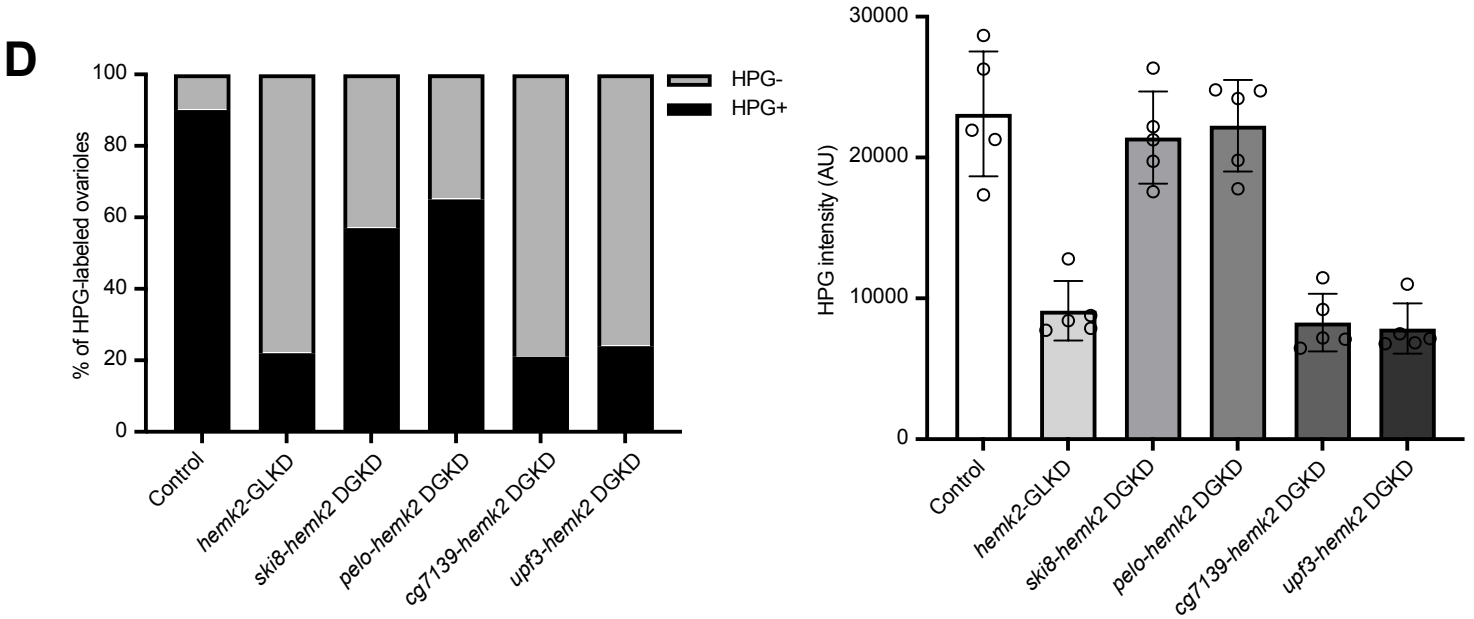
D
% of HPG-labeled ovarioles
100
80
60
40
20
0
HPG-
HPG+
Control
hemk2-GLKD
ski8-hemk2 DGKD
pelo-hemk2 DGKD
cg7139-hemk2 DGKD
upf3-hemk2 DGKD
HPG intensity (AU)
30000
20000
10000
0